
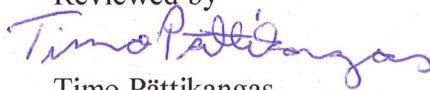
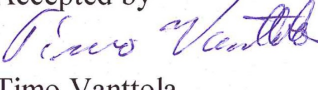


PORFLO modelling of the coolability of porous particle beds

Authors: Eveliina Takasuo, Ville Hovi, Mikko Ilvonen

Confidentiality: Public

Report's title PORFLO modelling of the coolability of porous particle beds	
Customer, contact person, address SAFIR2010 National Research Programme on Nuclear Power Plant Safety	Order reference 6/2010 SAF
Project name Hydrogen combustion risk and core debris coolability PORFLO-koulutus ja sovellus partikkelikeon jäähdytettävyyteen	Project number/Short name 41388/HYBCIS2 43216/PORFLO-koulutus
Author(s) Eveliina Takasuo, Ville Hovi, Mikko Ilvonen	Pages 41
Keywords PORFLO code, porous medium, STYX experiments, COOLOCE test facility, corium, particle bed coolability	Report identification code VTT-R-09376-10
Summary <p>PORFLO is a computational fluid dynamics code that utilizes porous medium approach for solving two-phase flow problems encountered in nuclear power plant thermal hydraulics. Models suitable for the simulation of porous core debris beds (particle beds) have been incorporated into the code. Using the new code version, the coolability and three-dimensional dryout behavior of this type of particle beds can be estimated. The flow and heat transfer solutions of the PORFLO code have been significantly revised during the work.</p> <p>Models have been generated of particle beds of two different geometries, a cylindrical and a conical particle bed. Experimental studies addressing both of these geometries have been conducted in the past or present experimental programs at VTT. In the present study, the focus is on the modelling of the new COOLOCE (Coolability of Cone) test facility. Results of the first PORFLO simulations and comparisons to the results given by the MEWA-2D code are presented. The different comparisons indicate that the PORFLO code is capable of reproducing the main features of the particle bed dryout process.</p>	
Confidentiality	Public
Espoo 11.1.2011 Written by  Reviewed by  Accepted by  Eveliina Takasuo Research Scientist Timo Pättikangas Senior Research Scientist Timo Vanttola Technology Manager	
VTT's contact address PO Box 1000, 02044-VTT, Finland	
Distribution (customer and VTT) SAFIR2010 and SAFIR2014 Reference Group 5 VTT: Timo Vanttola, Eija Karita Puska, Vesa Suolanen, Jarto Niemi, Stefan Holmström, Tuomo Kinnunen, Pekka H. Pankakoski, Tuomo Sevón, Tommi Kekki	
<i>The use of the name of the VTT Technical Research Centre of Finland (VTT) in advertising or publication in part of this report is only permissible with written authorisation from the VTT Technical Research Centre of Finland.</i>	

Contents

NOMENCLATURE.....	3
1 Introduction.....	4
2 The experimental facilities	5
3 The particle bed models	9
3.1 Heat transfer models.....	9
3.2 Friction models.....	13
3.2.1 Models without interfacial friction	14
3.2.2 Models including interfacial friction	15
3.2.3 List of PORFLO updates 2010.....	17
4 Simulation set-up.....	19
4.1 Cylindrical particle bed.....	19
4.2 The COOLOCE particle bed	22
5 Simulation results	25
5.1 Cylindrical particle bed.....	25
5.2 The COOLOCE particle bed	32
6 Conclusions.....	39
References	40

NOMENCLATURE

A	coefficient in the Ergun equation	[-]
B	coefficient in the Ergun equation	[-]
c_p	specific heat capacity	[J/kgK]
d_p	particle diameter	[m]
D_b	bubble diameter	[m]
g	gravitational acceleration	[m/s ²]
F	volumetric friction force	[N/m ³]
h	enthalpy	[J/kg]
j	superficial velocity	[m/s]
k	thermal conductivity	[W/mK]
K	permeability	[m ²]
K_r	relative permeability	[-]
L	length	[m]
m	model parameter	[-]
n	model parameter	[-]
p	pressure	[Pa]
Q	volumetric heat flux	[W/m ³]
s	saturation (liquid fraction)	[-]
T	temperature	[K]
u	velocity	[m/s]

Greek

α	void fraction	[-]
α_s	volume fraction of particles	[-]
α_h	volume fraction of heaters	[-]
Γ	phase change rate	[kg/m ³ s]
ε	porosity	[-]
η	passability	[m]
η_r	relative passability	[-]
μ	dynamic viscosity	[kg/ms]
ρ	density	[kg/m ³]

Subscripts

eff	effective
g	gas
h	heater
IF	interfacial
l	liquid
p	particle
PC	phase change
PL	particle-liquid
PG	particle-gas
r	relative
s	solid
sat	saturation, gas-liquid interface

1 Introduction

PORFLO is a computational fluid dynamics code that utilizes porous medium approach for solving problems encountered in nuclear power plant thermal hydraulics. In the present study, models that simulate the behavior of a decay heat-generating core debris bed have been created. At the Olkiluoto BWRs, the coolability and possible dryout of ex-vessel core debris bed is an important issue since the flooding of the lower drywell of the containment, and the subsequent discharge of corium into the deep water pool, is a key part of severe accident management strategy. Heat has to be removed from the solidified corium in order to stabilize the material and prevent possible re-melting.

The application of the PORFLO code to particle bed coolability was included in the code development during 2010, simultaneously with the assembly of the new COOLOCE experimental facility. Using the COOLOCE facility particle beds of different geometries, such as heap-like (conical) set-ups, may be investigated. The planned COOLOCE test series continues the work done within the STYX test programme (see e.g. Takasuo et al. 2010) which examined coolability in cylindrical particle beds.

In a cylindrical particle bed, the coolability (dryout behavior) is usually governed by top flooding flow configuration. In these cases, one-dimensional models are often considered adequate for predicting dryout power. In the conical configuration, multi-dimensional flows from the sides of the particle bed are present, and they play a significant role in the dryout process. Thus, multi-dimensional modelling is needed in the case of complex particle bed geometries.

Several friction and heat transfer models suitable for the particle bed application have been selected based on previous analysis by e.g. Schmidt (2004) and Bürger et al. (2006) and incorporated into the PORFLO code. For the most part, these models are the same as used in the MEWA-2D severe accident analysis code, developed by Stuttgart University (Bürger et al. 2006). The approach used in the MEWA-2D code has been used as a starting point for the programming of the PORFLO heat transfer models with the permission given by the MEWA-2D developers.

It should be noted that during this application-specific work, the PORFLO code has gone through significant revisions within the frame of the overall code development. The solutions of the basic conservation equations have been revised and attention has been paid to improving the convergence of the numerical methods. This is a long-term effort that aims at code improvement independently of the application. More information can be found in Ilvonen et al. (2010).

In this report, brief descriptions of the STYX and COOLOCE test facilities and a more detailed description of the computational models are presented. The results of the first PORFLO 3D simulations of the cylindrical and conical particle beds are included. The PORFLO results are compared to the results obtained by MEWA-2D, and a preliminary comparison to the first COOLOCE experimental results is also given.

2 The experimental facilities

The coolability of cylindrical porous beds that consist of irregular particles has been investigated within the STYX test programme. The experiments were conducted between 2001 and 2008. The test bed consists of relatively small irregular alumina particles arranged in a cylindrical configuration that is 30 cm in diameter and 60 cm in height in the basic test configuration. The schematic of the main components of the STYX facility is presented in Fig. 1. The particle bed for which the dryout power and location is measured is installed inside a custom-made pressure vessel that allows testing up to 7 bar. The internal heat generation, which in reactor scenarios results from the decay of the fission products, is achieved by resistance heating.

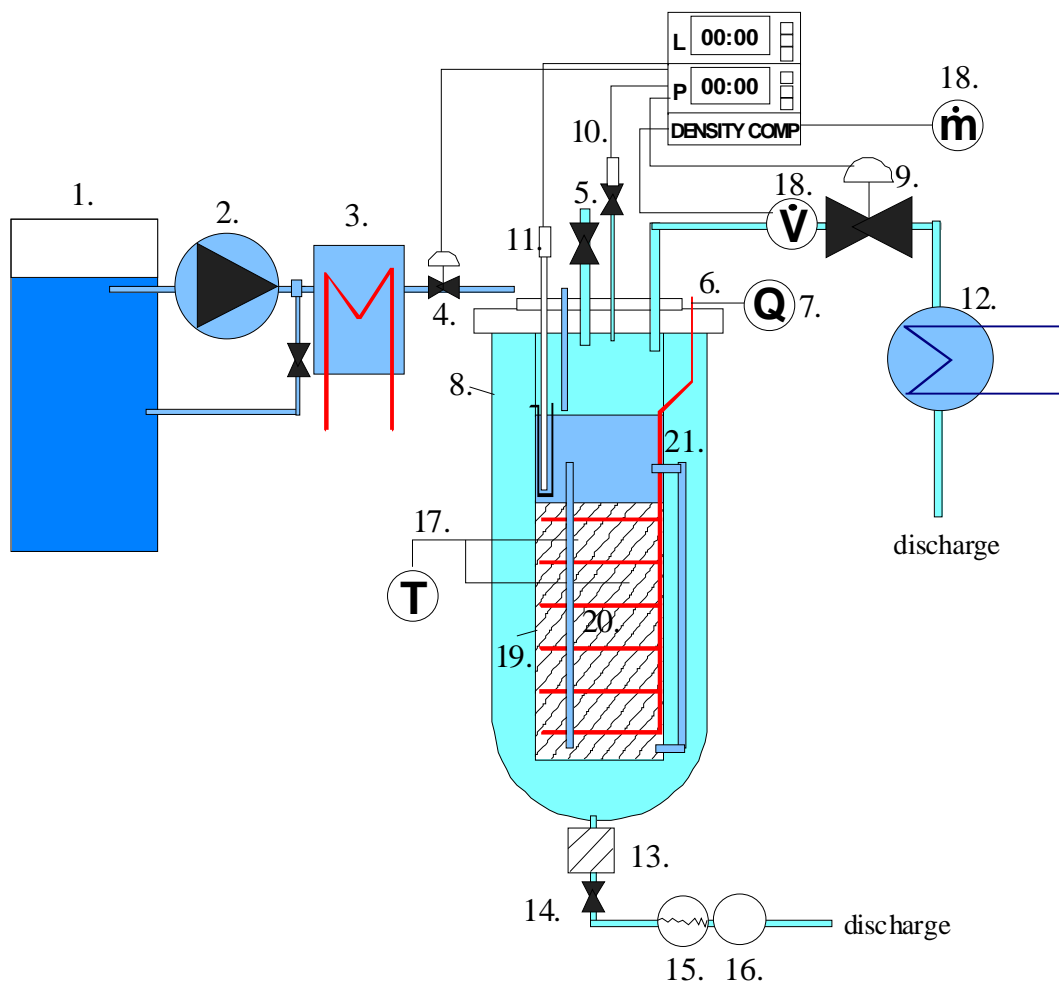


Fig. 1. The schematic of the STYX facility. Figure 1. Schematic of the STYX test facility: 1) feedwater tank, 2) feedwater pump, 3) pre-heater 4) feed water valve, 5) pressure gauge (measurement), 6) heating element, 7) power input and measurement, 8) pressure vessel 9) pressure valve (control), 10) pressure gauge (control), 11) water level indicator (control), 12) condenser, 13) impurities sifter, 14) valve (condensate line), 15) condensate level indicator, 16) condensate separator, 17) thermocouples (measurement), 18) flow meter (mass or energy flow), 19) inner vessel, 20) test bed, 21) downcomers.

The COOLOCE (Coolability of Cone) test facility was designed in 2009 and assembled in 2010 for investigations of dryout power in a conical particle bed within the frame of the HYBCIS and HYBCIS2 projects in the SAFIR2010 research programme. A cylindrical test bed will be assembled later, and is used as a reference for the conical test bed. The feed water and steam removal systems as well as the power supply are in principle the same as the ones in the STYX test but the pressure vessel and its interior have been replaced by completely new components.

Detailed descriptions of the STYX test rig can be found in the publication by Lindholm et al. (2006) and Takasuo et al. (2010). The description of the COOLOCE facility is found in the report by Takasuo et al. (2010). Table 1 summarizes the different specifications of the STYX and COOLOCE test facilities. The presented COOLOCE specifications are those that were used in the start-up phase of the test rig.

Table 1. Comparison of the STYX and COOLOCE particle bed coolability test facilities.

	STYX	COOLOCE
Pressure range	1-7 bar	1-7 bar
Particle bed geometry	Cylindrical	Conical (flexible)
Flow condition	Top inflow (downcomers possible)	Multi-dimensional inflow
Porosity (approx.)	0.37	0.37
Particle size distribution	0.25 - 10.0 mm	0.8 - 1.0 mm
Particle shape	Irregular	Spherical
Particle material	Al ₂ O ₃	ZrO ₂ 65% / SiO ₂ 35%
Heating method	Wire resistance elements in nine horizontal levels	137 vertical custom-length cartridge heaters
Nominal maximum power	63 kW	63 kW
Temperature transducers	50 K type thermocouples	69 K type thermocouples
Visual observations	-	3 sightglasses, video recorder

A photograph of the COOLOCE pressure vessel is shown in Fig. 2(a). The pressure vessel has a volume of 270 dm³ and inner diameter of 600 mm. The vessel is equipped with three sightglasses, one on the upper head to provide lighting and two in the walls at 135° division. Cameras can be mounted to the sightglasses to monitor the particle bed.

The COOLOCE particle bed consists of ceramic spheres that are being held in conical shape by a dense wire net. The particle bed is heated by resistance heating system using 6.3 mm heaters of different lengths which are installed in a “square mesh” at 3 mm distance from each other. The configuration aims at achieving a uniform temperature distribution within the test bed. The nominal maximum

power of the heaters is 55 kW. Fig. 2(a) and (b) demonstrate the heating arrangements inside the conical heap of particles.

K type thermocouples are installed between the heaters at different heights in the test bed. The thermocouples are used to determine dryout heat flux and its location: an increase from saturation temperature somewhere in the bed interior indicates local dryout. The heaters and thermocouples are connected through the pressure vessel bottom that contains a total of 215 tapered holes for the different connections.

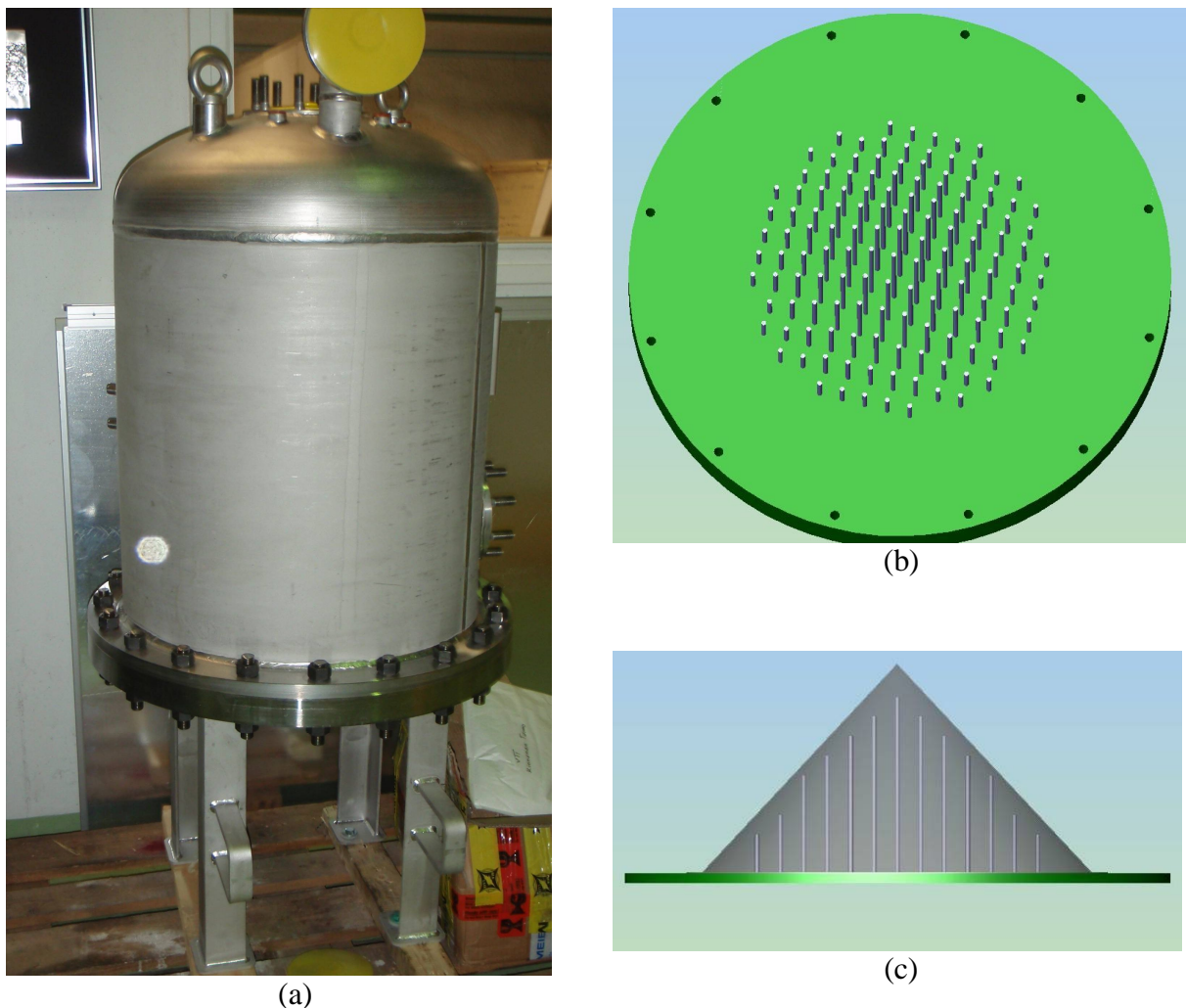


Fig. 2. The COOLOCE pressure vessel (a) and the conceptual design of the heating configuration (b, c).

The test procedure is similar in both COOLOCE and STYX experiments. In the beginning of the experiments the vessel is filled with demineralised water that is heated up to the saturation temperature at the respective pressure. After this first steady-state has been established, a stepwise power increase is conducted until local dry-out is observed. Sufficient waiting time (20-30 minutes) is applied between the power increments in order to see whether the particle bed stabilizes to a coolable state or dryout is reached. The numerical simulations which aim to determine the dryout power follow a similar logic: We need to find out 1) the

heating power at which the particle bed just stays coolable and 2) the minimum heating power that leads to dryout (from which dryout heat flux or volumetric dryout power can be calculated).

3 The particle bed models

The particle bed model in the PORFLO code is based on the 3D solution of the conservation equations for mass, momentum and energy. The closure models for friction and heat transfer have been selected from the literature. The friction models are based on well-known approaches used to simulate porous media. The selection of many of the heat transfer models in the present code version is based on the approaches used in MEWA (code distribution of 2008) with the permission of the code developers. The models are described in the following sections.

3.1 Heat transfer models

In this Section, a review of the heat transfer models incorporated into PORFLO for the particle bed calculations is given. The energy conservation equations for liquid (Eq.1) and gas (Eq.2) have the following form:

$$\frac{\partial [\varepsilon(1-\alpha)\rho_l h_l]}{\partial t} + \nabla \cdot [\varepsilon(1-\alpha)\rho_l h_l \mathbf{u}_l] = Q_{h,l} + Q_{s,l} - Q_{l,sat} - \Gamma h_l \quad (1)$$

$$\frac{\partial (\varepsilon\alpha\rho_g h_g)}{\partial t} + \nabla \cdot (\varepsilon\alpha\rho_g h_g \mathbf{u}_g) = Q_{h,g} + Q_{s,g} - Q_{g,sat} + \Gamma h_g \quad (2)$$

where h_g is vapor enthalpy [J/kg] and h_l is liquid enthalpy [J/kg]. On the right hand side $Q_{h,l}$ is the volumetric heat flux from heaters to liquid [W/m^3], $Q_{s,l}$ is the heat flux from the solid particles to liquid [W/m^3], $Q_{l,sat}$ is the heat flux from the liquid phase to the interface of gas and liquid [W/m^3] and Γh_l the enthalpy flux resulting from boiling [$\text{J}/\text{m}^3\text{s}$]. The heat fluxes Q for the gas phase in Eq. 2 correspond to those of the liquid phase. Porosity is denoted by ε and void fraction by α .

The most important heat transfer mechanism inside the particle bed is (usually) boiling. Assuming steady-state conditions, the heat generated by the solid phase is consumed by the phase change of the coolant water that is in contact with the solid particles. Convection from the solid particles plays an increasing role only after local dryout when there is no liquid available in the bed interior and the particles are in contact with the vapour phase.

In investigating the effect of the experimental heating arrangement, as compared to the homogenous heating present in reactor applications, it is useful to estimate the effectiveness of heat transfer from the heating elements into the test bed. This should take into account the heat transfer inside the solid matrix and across the local inhomogeneity of the bed geometry formed between the heater surfaces and the bulk of particles. The heat transfer correlations selected for the different convective, conductive and boiling mechanisms in the porous bed aim at reproducing the experimental situation with a high accuracy. This also facilitates the modelling of power plant scenarios in a detailed fashion.

The model of the Loviisa steam generator (Hovi and Ilvonen, 2010) was used as a starting point for the heat transfer solution of the particle bed model. In this case the temperature of the tubes was taken as a boundary condition. In the COOLOCE model, however, the solid temperature distribution has to be solved while heating power is the control parameter. The heaters are taken into account separately from the bed particles. This way, we can specify the heat source directly to the heaters, and examine heat transfer from the heaters to the particles.

Heat conduction equations are solved for the heaters and porous particles, as well as the heat flux from the heaters to the particles. The presence of the fluid phases in the pores of the particle bed is implicitly included in the effective thermal conductivity. The effective thermal conductivity is calculated according to the Imura and Takegoshi (1973) model combined to the Vortmeyer (1978) radiation model. The heat equations for the heaters and solid particles are

$$\varepsilon_s \rho_s c_{p,s} \frac{\partial T_s}{\partial t} + \nabla \cdot (-k_{\text{eff}} \nabla T_s) = Q_{h,s} - Q_{s,l} - Q_{s,g} - Q_{s,\text{sat}} \quad (3)$$

$$\varepsilon_h \rho_h c_{p,h} \frac{\partial T_h}{\partial t} + \nabla \cdot (-k_h \nabla T_h) = Q_{\text{source}} - Q_{h,s} - Q_{h,l} - Q_{h,g} - Q_{h,\text{sat}} \quad (4)$$

The thermal conductivities k_{eff} and k_h [W/mK] are given for the bulk of particles and the heaters, respectively. In Eq. (3) $Q_{s,h}$ is the conduction heat flux from the particles to the heaters, $Q_{s,l}$ and $Q_{s,g}$ are the heat fluxes from particles to the fluid phases and $Q_{s,\text{sat}}$ is the heat flux to the interface of gas and liquid (boiling). In Eq. (4) Q_{source} is the heat flux generated by the heaters, $Q_{h,s}$ is the conduction heat flux from the heaters to the particles, $Q_{h,l}$ and $Q_{h,g}$ are the heat fluxes from heaters to the fluid phases and $Q_{h,\text{sat}}$ is the heat transferred directly to boiling. ε_s denotes the volume fraction occupied by the particles and ε_h the fraction of heaters.

The heat transfer mechanisms in the modelled case are illustrated in Fig. 3 (next page). The flow regimes (indicative) in which the different heat transfers are active from bottom to top in the figure are single-phase liquid, bubbly flow, droplet flow and single-phase gas. Accordingly, the heat fluxes between the fluid and the interface are given separately for three flow regimes: bubbly, droplet and transition between the two. Boiling heat flux at the particle and heater surfaces is divided to pool and film boiling and a transition regime. Note that, for the sake of clarity, the transition regime heat fluxes are omitted from the illustration of Fig. 3 and only one boiling heat flux for each of the solid phases (heater and particles) is indicated.

The mass transfer rate is obtained by dividing the heat fluxes directed to the interface of gas and liquid with the latent heat of evaporation:

$$\Gamma = \frac{Q_{s,\text{sat}} + Q_{h,\text{sat}} + Q_{l,\text{sat}} + Q_{g,\text{sat}}}{h_{l,g}} \quad (5)$$

This is present as a source term in the mass and energy balance of gas and liquid. To clarify the general picture further, the heat fluxes and the references to the original models are listed in Table 2 and Table 3. In the calculation of the heat transfer coefficients, the applied model is selected based on the flow regime. The presently available models for the different regimes are given in the tables. Table 2 lists the heat fluxes from the solid phases to the fluids and between the two solids. Table 3 presents the heat fluxes to the interface of gas and liquid, based on which the boiling rate is calculated for both the fluid and solid “side”. The procedure of calculating the heat transfer rates in PORFLO is shown in Fig. 4.

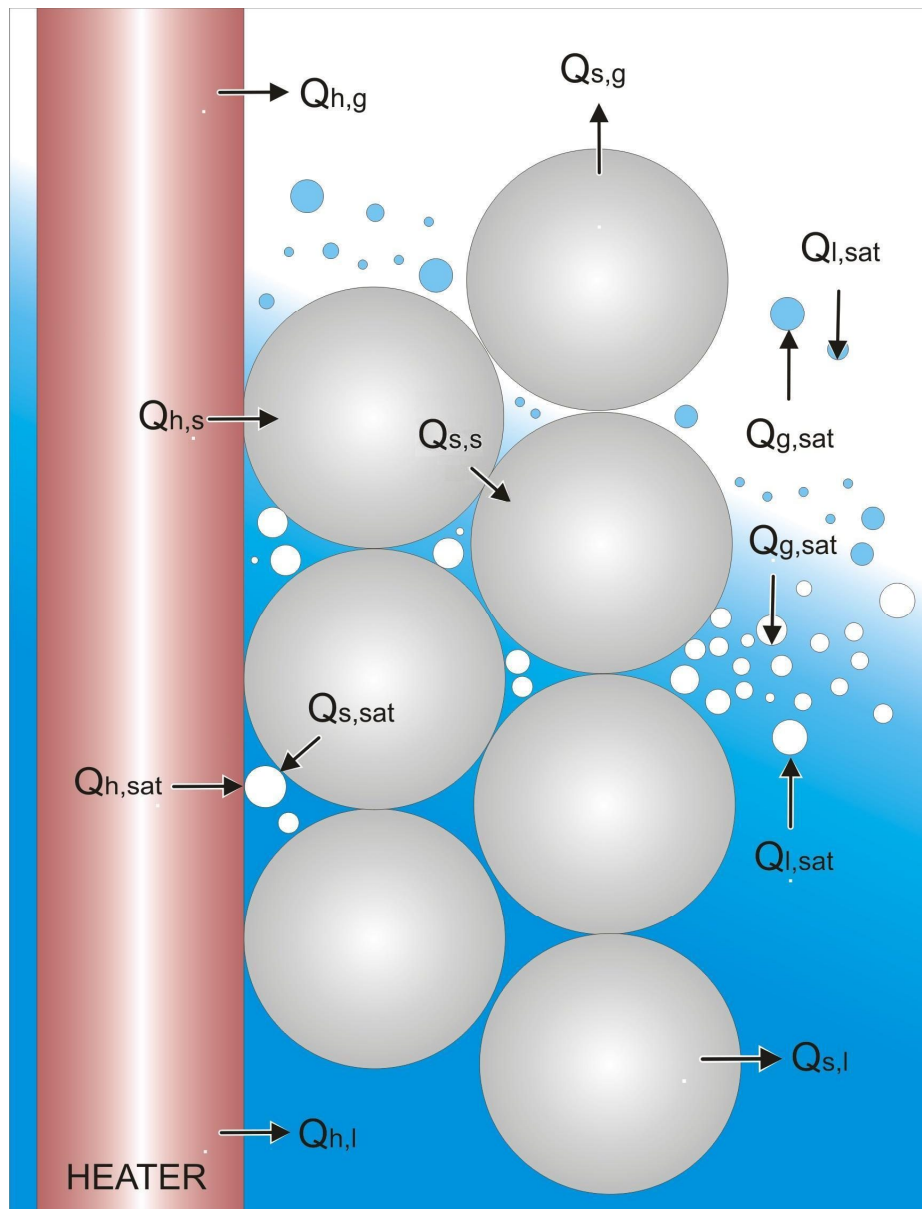


Fig. 3. Heat fluxes in the porous medium configuration which includes two-phase flow and the local heating method used in experimental facilities.

Table 2. The conductive and convective heat fluxes from the solid phases and the corresponding heat transfer models in the PORFLO code.

Heat transfer mechanisms	Notation	Model reference
Particles to gas convection	$Q_{s,g}$	MEWA default model (Buck et al. 2009)
Heaters to gas convection	$Q_{h,g}$	
Particles to liquid convection	$Q_{s,l}$	
Heaters to liquid convection	$Q_{h,l}$	
Heaters to particles conduction	$Q_{h,s}$	3D conduction equation
Particles to particles conduction	$Q_{s,s}$	

Table 3. The heat fluxes and heat transfer models that contribute to the mass transfer rate (boiling) in the PORFLO code. The applied model depends on the flow regime.

Solid-interface heat fluxes		
Heat transfer mechanisms	Notation	Model reference
Particles to interface pool boiling	$Q_{s,sat}$	Rohsenow (1952)
Heaters to interface pool boiling	$Q_{h,sat}$	
Particles to interface film boiling	$Q_{s,sat}$	Lienhard and Dhir (1973)
Heaters to interface film boiling	$Q_{h,sat}$	
Particle to interface transition boiling	$Q_{s,sat}$	Weighting function
Heaters to interface transition boiling	$Q_{h,sat}$	
Fluid-interface heat fluxes		
Heat transfer mechanisms	Notation	Model reference
Liquid to interface in bubbly flow	$Q_{l,sat}$	Lee and Ryley (1968)
Gas to interface in bubbly flow	$Q_{g,sat}$	
Liquid to interface in droplet flow	$Q_{l,sat}$	
Gas to interface in droplet flow	$Q_{g,sat}$	
Liquid to interface transition regime	$Q_{l,sat}$	Weighting function
Gas to interface transition regime	$Q_{g,sat}$	

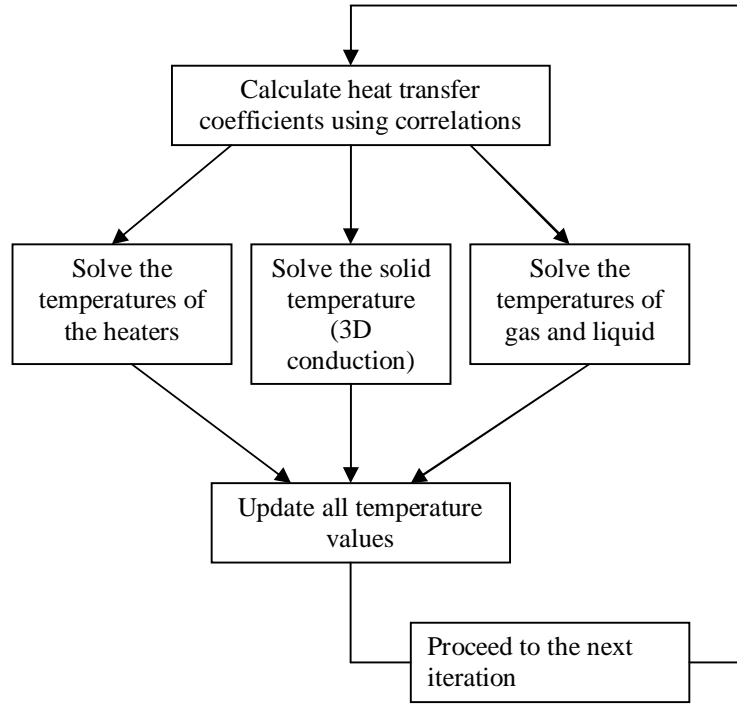


Fig. 4. Heat transfer calculation steps in PORFLO.

3.2 Friction models

In the case of dense porous particle beds, the flow is dominated by frictional forces between the three phases. These appear as source terms in the momentum equations. PORFLO solves the following basic momentum equations for liquid and gas phases:

$$\frac{\partial [\varepsilon(1-\alpha)\rho_l \mathbf{u}_l]}{\partial t} + \nabla \cdot \{ [\varepsilon(1-\alpha)\rho_l \mathbf{u}_l] \otimes \mathbf{u}_l \} = -\varepsilon(1-\alpha)\nabla p + \varepsilon(1-\alpha)\nabla \cdot \mathbf{T} + \varepsilon(1-\alpha)\rho_l \mathbf{g} + \mathbf{F}_{PC} + \mathbf{F}_{IF} + \mathbf{F}_{PL} \quad (6)$$

$$\frac{\partial (\varepsilon\alpha\rho_g \mathbf{u}_g)}{\partial t} + \nabla \cdot [(\varepsilon\alpha\rho_g \mathbf{u}_g) \otimes \mathbf{u}_g] = -\varepsilon\alpha\nabla p + \varepsilon\alpha\nabla \cdot \mathbf{T} + \varepsilon\alpha\rho_g \mathbf{g} - \mathbf{F}_{PC} - \mathbf{F}_{IF} + \mathbf{F}_{PG} \quad (7)$$

where \mathbf{F}_{IF} is the interfacial friction force [N/m³], ε is porosity, \mathbf{F}_{PC} is the momentum transfer due to phase change [N/m³] and \mathbf{F}_{PL} and \mathbf{F}_{PG} represent the frictional forces [N/m³] between the fluids and the solid matrix.

These friction terms are case-dependent. For the particle bed case, we need the drags between the gas and solid, and liquid and solid phases as well as the interfacial friction. The role of interfacial friction is pronounced in the case of multi-dimensional flows that are present in complex geometries. For a classical particle bed that consists of a column into which water infiltration is from the top (or bottom) only, models without explicit consideration of interfacial friction are adequate. Both the classical model and a model with explicit interfacial friction have been implemented and tested.

3.2.1 Models without interfacial friction

The friction models for the three phases available in PORFLO before the present work were adjusted for flows across tube bundles in the simulations of Loviisa steam generator and the fuel rods of the BFBT benchmark. In a densely packed particle bed consisting of small particles the order of mm, however, the pressure loss is significantly greater than in typical tube systems. The pressure loss in porous media can be estimated using the Ergun equation:

$$\frac{\Delta p}{L} = \frac{\mu}{K} j + \frac{\rho}{\eta} |j| j - \rho g \quad (8)$$

The parameters K and η are called permeability and passability and they are calculated by

$$K = \frac{\varepsilon^3 d_p^2}{A(1-\varepsilon)^2}, \quad A = 150 \quad (9)$$

$$\eta = \frac{\varepsilon^3 d_p}{B(1-\varepsilon)}, \quad B = 1.75 \quad (10)$$

The velocity j is superficial velocity, i.e. the velocity that corresponds to the total mass flow rate across the particle bed. The phase velocities can be obtained by dividing the superficial velocity by the fraction of the phase in the system. Two-phase flows are taken into account by introducing relative permeability and passability for the gas phase

$$K \rightarrow K K_{rg}(\alpha)$$

$$\eta \rightarrow \eta \eta_{rg}(\alpha)$$

and for the liquid phase

$$K \rightarrow K K_{rl}(1-\alpha)$$

$$\eta \rightarrow \eta \eta_{rl}(1-\alpha)$$

The relative permeability and passability are parameters that quantify the effect of the reduced flow area of each phase, and separate the pressure drop of the two phases. Usually, these are defined as $K_{rg} = \alpha^n$, $K_{rl} = (1-\alpha)^n$ and $\eta_{rg} = \alpha^m$, $\eta_{rl} = (1-\alpha)^m$. Inserting the aforementioned expressions into the Ergun equation an estimate of the two-phase flow pressure drop is obtained:

$$\frac{\Delta p}{L} = \frac{\mu A (1-\varepsilon)^2}{\varepsilon^3 d_p^2 \alpha^n} j + \frac{\rho B (1-\varepsilon)}{\varepsilon^3 d_p \alpha^m} |j| j - \rho g \quad (11)$$

The volumetric friction force is

$$F = \frac{\mu A(1-\varepsilon)^2}{\varepsilon^3 d_p^2 \alpha^n} j + \frac{\rho B(1-\varepsilon)}{\varepsilon^3 d_p \alpha^m} |j| j \quad (12)$$

This can be written for both fluid phases (\mathbf{F}_{PL} and \mathbf{F}_{PG}) and inserted into the momentum equations of gas and liquid. The powers m and n are chosen based on experiments (see e.g. Schmidt, 2004). The common approaches are listed in Table 4.

Table 4. Exponents for relative permeability (n) and passability (m) according to different experiments.

	n	m
Lipinski	3	3
Reed	3	5
Theofanous	3	6

In this model, the interfacial friction is implicitly included in the relative permeability and passability, and the term \mathbf{F}_{IF} is omitted from the momentum equations which yields:

$$\frac{\partial [\varepsilon(1-\alpha)\rho_l \mathbf{u}_l]}{\partial t} + \nabla \cdot \{ [\varepsilon(1-\alpha)\rho_l \mathbf{u}_l] \otimes \mathbf{u}_l \} = -\varepsilon(1-\alpha)\nabla p + \varepsilon(1-\alpha)\nabla \cdot \mathbf{T} \quad (13)$$

$$+ \varepsilon(1-\alpha)\rho_l \mathbf{g} + \mathbf{F}_{PL} + \mathbf{F}_{PC}$$

$$\frac{\partial (\varepsilon\alpha\rho_g \mathbf{u}_g)}{\partial t} + \nabla \cdot [(\varepsilon\alpha\rho_g \mathbf{u}_g) \otimes \mathbf{u}_g] = -\varepsilon\alpha\nabla p + \varepsilon\alpha\nabla \cdot \mathbf{T} + \varepsilon\alpha\rho_g \mathbf{g} + \mathbf{F}_{PG} - \mathbf{F}_{PC} \quad (14)$$

3.2.2 Models including interfacial friction

It is well established experimentally and analytically (e.g. Tutu et al. 2004) that in order to capture the pressure gradient inside the porous bed correctly, it is necessary to include a separate model for interfacial friction. It was chosen to use the Tung and Dhir model (1988) including the modifications for smaller particle size range proposed by Schmidt (2004). The implementation of the models into PORFLO utilizes the presentation given by Buck et al. (2009).

In the modified Tung and Dhir model, the friction forces depend on the flow regime through separate expressions for relative permeability and passability for bubbly, slug and annular flow. The correlations for the relative permeability and passability of the fluid-particle drags and for the interfacial friction \mathbf{F}_{IF} in the different flow regimes are presented in Table 5. The bubble diameters used in bubbly and slug flow regimes are given in Table 6, and the void fraction boundaries below which the different flow regimes are applicable in Table 7.

Table 5. Summary of the Tung and Dhir two-phase friction model.

Friction and flow regime	Correlation
Liquid-solid (all regimes)	$K_{rl} = \eta_{rl} = (1 - \alpha)^3$
Gas-solid (bubbly and slug flow)	$K_{rg} = \left(\frac{1 - \varepsilon}{1 - \varepsilon \alpha} \right)^{4/3} \alpha^4$ $\eta_{rg} = \left(\frac{1 - \varepsilon}{1 - \varepsilon \alpha} \right)^{2/3} \alpha^4$
Gas-solid (transition)	$W(\xi) = \xi^2(3 - 2\xi)$ $\xi = \frac{\alpha - \alpha_i}{\alpha_{i+1} - \alpha_i}$
Gas-solid (annular flow)	$K_{rg} = \left(\frac{1 - \varepsilon}{1 - \varepsilon \alpha} \right)^{4/3} \alpha^3$ $\eta_{rg} = \left(\frac{1 - \varepsilon}{1 - \varepsilon \alpha} \right)^{2/3} \alpha^3$
Gas-liquid (bubbly flow)	$F_{IF} = 18\alpha \frac{\mu_l}{D_b^2} (1 - \alpha) j_r + 0.34(1 - \alpha)^3 \alpha \frac{[(1 - \alpha)\rho_l + \alpha\rho_g]}{D_b \varepsilon} (1 - \alpha)^2 j_r j_r$
Gas-liquid (bubbly-slug transition)	$W(\xi) = \xi^2(3 - 2\xi)$ $\xi = \frac{\alpha - \alpha_i}{\alpha_{i+1} - \alpha_i}$
Gas-liquid (slug flow)	$F_{IF} = 5.21\alpha \frac{\mu_l}{D_b^2} (1 - \alpha) j_r + 0.92(1 - \alpha)^3 \alpha \frac{[(1 - \alpha)\rho_l + \alpha\rho_g]}{D_b \varepsilon} (1 - \alpha)^2 j_r j_r$
Gas-liquid (slug-annular transition)	$W(\xi) = \xi^2(3 - 2\xi)$ $\xi = \frac{\alpha - \alpha_i}{\alpha_{i+1} - \alpha_i}$
Gas-liquid (annular flow)	$F_{IF} = \frac{\mu_g}{KK_{rg}} (1 - \alpha) j_r + (1 - \alpha) \alpha \frac{\rho_g}{\eta \eta_{rg}} j_r j_r$
Gas-liquid (modified annular)	$F_{IF} = \left(\frac{\mu_g}{KK_{rg}} (1 - \alpha) j_r + (1 - \alpha) \alpha \frac{\rho_g}{\eta \eta_{rg}} j_r j_r \right) (1 - \alpha)^2 \begin{cases} \left(\frac{d_p}{6 * 10^{-3}} \right)^2 : d_p < 6mm \\ 1 : d_p > 6mm \end{cases}$

Table 6. The expressions of bubble diameter in the original and modified Tung and Dhir models.

Bubble diameter	
Original model (Tung and Dhir, 1988)	$D_b = 1.35 \sqrt{\frac{\sigma}{g(\rho_l - \rho_g)}}$
Modified model (Schmidt, 2004)	$D_b = \min \left(1.35 \sqrt{\frac{\sigma}{g(\rho_l - \rho_g)}}, 0.41d_p \right)$

Table 7. The void fraction boundaries of the different flow regimes in the original and modified Tung and Dhir models.

Flow regime	Void fraction upper limits for the original model	Void fraction upper limits for the modified model (small particles)
Bubbly flow	$\alpha_1 = \min \{ 0.3, 0.6 \cdot (1 - \gamma)^2 \}$	$\alpha_1^m = \frac{\pi / 6}{5} (d_p - 8mm) + \alpha_1$
Transition from bubbly flow to slug flow	$\alpha_2 = \frac{\pi}{6}$	$\alpha_2^m = \frac{\pi / 6}{5} (d_p - 8mm) + \alpha_2$
Slug flow	$\alpha_3 = 0.6$	$\alpha_3^m = \frac{\pi / 6}{5} (d_p - 8mm) + \alpha_3$
Transition from slug flow to annular flow	$\alpha_4 = \frac{\pi \sqrt{2}}{6}$	$\alpha_4^m = \frac{\pi / 6}{5} (d_p - 6mm) + \alpha_4$
Annular flow	$\alpha_5 = 1.0$	$\alpha_5^m = 1.0$

3.2.3 List of PORFLO updates 2010

The following list summarized the updates that have been done to the code during the development work of the particle bed model.

1. The particle bed geometry routine has been implemented into the code
2. The heat transfer solution routine has been modified so that the heating power may be given as input value
3. The heat transfer models for the particle bed application have been included (the state-of-the-art models utilized in the MEWA code were taken as the starting point)

4. The particle bed friction models were included (the state-of-the-art models utilized in the MEWA code were taken as the starting point)
5. The possibility to use different friction models for the particle bed and the pool region have been included, making it possible to model and investigate the pool dynamics in detail
6. A heat transfer model for pure conduction has been implemented in order to examine the heat transfer inside and between different types of solids
7. A possibility for explicit temperature solution has been added which improved convergence of the particle bed calculations
8. Several additional output options have been included
9. The possibility to create animations of the results by the StarNode visualization tool have been included

4 Simulation set-up

Two different flow configurations are investigated in the simulations:

- 1) A cylindrical reference particle bed with top flooding
- 2) A conical particle bed (a model of the COOLOCE facility)

The first case approximates the flow configuration of the STYX experiments while the second case estimates the behavior of the COOLOCE, or a conical (heap-like), particle bed. The cases are modelled by both the PORFLO and MEWA codes. In order to make the comparison of the two codes possible, the simulation parameters are selected to be as similar as possible in the two codes.

However, it should be noticed that, here, the aim of the top-flooding simulations is not to produce a detailed model of the STYX experimental set-up but to point out and identify the differences between the codes, with the focus being on PORFLO development and validation. Previous, comprehensive studies indicate that the MEWA model is capable of reproducing the results of the STYX top flooding experiments with good accuracy by using models based on the Ergun equation and appropriate selection of parameters (Takasuo et al. 2010).

4.1 Cylindrical particle bed

A subroutine has been implemented in the PORFLO code that generates a full 3D Cartesian grid for the calculation cases. In the base case the grid has 21x21x28 cells. The cell size is 30mm x 30 mm x 30 mm. A 2D model that has the same cell size has been generated using the MEWA code, resulting in a 10 x 12 grid. In addition, a denser grid of 60 x 72 cells has been generated in order to distinguish the possible grid effect and to better evaluate the dryout power. In MEWA, the grid generation is done by the standard input file of the code.

The PORFLO and MEWA grids for the top flooding cases are illustrated in Fig. 5 and Fig. 6, respectively. The fluid volume inside the pressure vessel is modelled in the PORFLO case, and a possibility to include different friction models for the porous bed and the “open” water pool is available. Thus, the pool dynamics can be taken into account in PORFLO. In the MEWA model, the pool is modelled by the same friction models as the porous bed (with the approximation of free flow conditions done by adjusting the porosity and particle size when necessary). This means that there is no separate consideration of the water pool from the particle bed in MEWA, resulting in a rather artificial representation of the fluid flow in the water region.

Pressure boundary conditions with the possibility of liquid inflow are given at the top of the computational domain in both the PORFLO and MEWA cases. The other boundaries are adiabatic and no flow is allowed through them.

In PORFLO, porosity in each cell is given according to the volumes occupied by the different structures in each cell, which results in smoothing of sharp porosity changes at the interfaces of the fluid and the structures. Because the ratio of heater diameter to the cells size is roughly 6 mm / 30 mm and one heater is contained in each cell column, the heat source is effectively homogenous in the particle bed cells in the present grid.

Contrary to PORFLO, in MEWA the grid is built in such a way that the boundary of the structure coincides with the cell boundary. Porosity for each cell is stated in the input file. If smoothing of the boundaries is required (e.g. for numerical stability of the model) this may be done by manually setting the porosity in the input file.

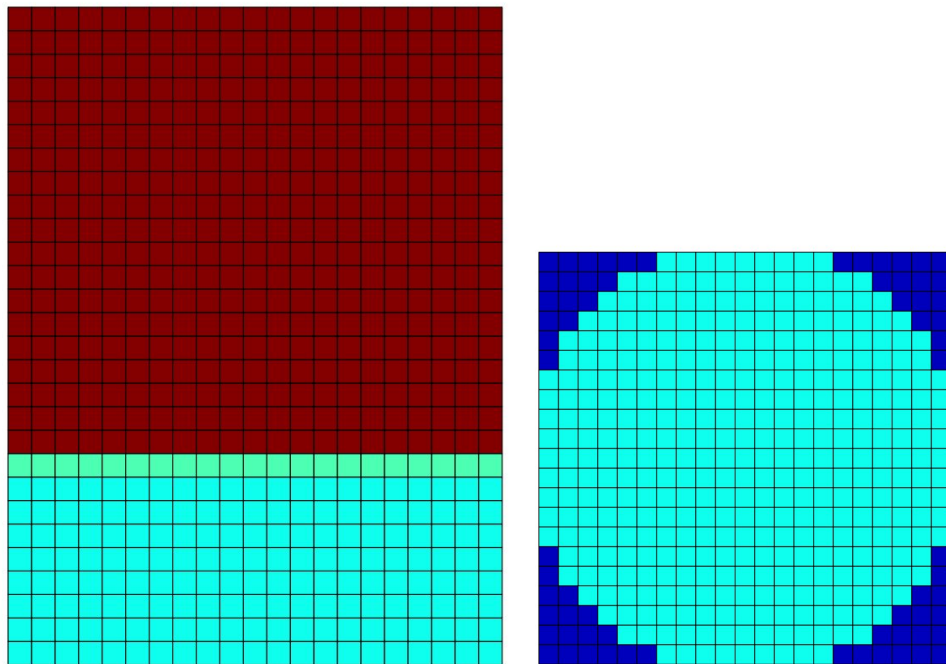


Fig. 5. Vertical central cross-section (left) and horizontal cross-section at the level of the particle bed (right) of the PORFLO grid for the top flooding calculations.

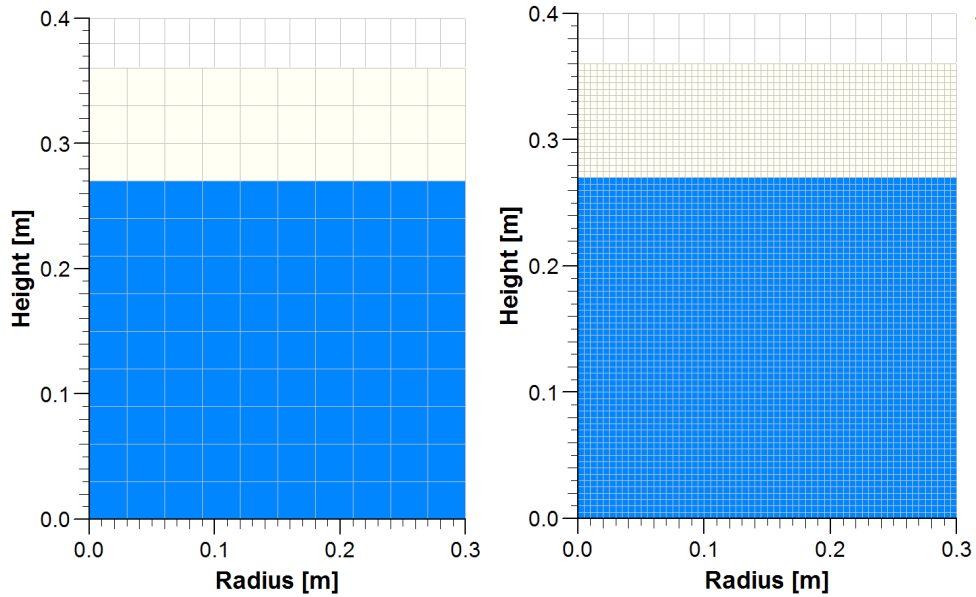


Fig. 6. The MEWA 2D grids for the top flooding calculations. The blue area is the particle bed (37% porosity).

The important physical parameters that govern the dryout behavior of porous particle beds - and usually contain the largest uncertainties - are porosity and particle size. In the calculations, default values of 0.8 mm for particle size and 0.37 for porosity were assumed. The simulation parameters for the codes are summarized in Table 8.

The ambient pressure in all the presented simulations is taken to be 1 bar. This is a reference pressure aiming for an easy comparison of the different simulations. It should be noticed that in the COOLOCE and STYX experiments, several pressure levels have been investigated, and the actual pressure may vary depending on the steam flow and the capabilities of the control system.

Table 8. The simulation set-up for the PORFLO and MEWA calculations of the cylindrical particle bed.

Simulation parameter	PORFLO (2010)	MEWA (2008)
Coarse grid	21 x 21 x 28 (3D)	10 x 12 (2D)
Dense grid	-	60 x 72
Particle bed height	270 mm	270 mm
Particle bed radius	306.5 mm	300 mm
Particle bed volume	0.07969 m ³	0.07634 m ³
Cell size	30 mm	30 mm
Porosity	~0.36 (calculated based on structure dimensions)	0.37 (given as input)
Pool porosity	0.90	0.99
Particle size	0.8 mm	0.8 mm
Pool particle size	2.0 mm	10.0 mm
Porosity transition zone from pool to particles	Yes	No
Porous friction model	Reed	Reed
Pool friction model	Reed	Reed
Upper boundary condition	Pressure, liquid flow only	Pressure, liquid flow only
Wall boundary conditions	Adiabatic, no flow-through	Adiabatic, no flow-through
Heat conductivity model	Imura-Takegoshi/Vortmeyer	Imura-Takegoshi/Vortmeyer
Heated fraction of the porous bed	~100%	100%
Simulation time-step	0.02-0.05 s	Controlled by the code

4.2 The COOLOCE particle bed

The PORFLO cell size and number in the conical particle bed are similar to those of the cylindrical bed. The PORFLO 3D grid is illustrated in Fig. 7 and the MEWA 2D grid in Fig. 8. The conical reference MEWA case is slightly different from the cylindrical case with its 11 x 12 cells grid. Similarly as in the cylindrical case a denser MEWA grid is also created in order to better approximate realistic values of dryout power. The dense grid has 25 x 89 cells.

The parameter selections are the same as in the cylindrical case. The models and parameters are listed in Table 9. For the particle bed friction, the modified Tung and Dhir model is used as explained in Chapter 3.

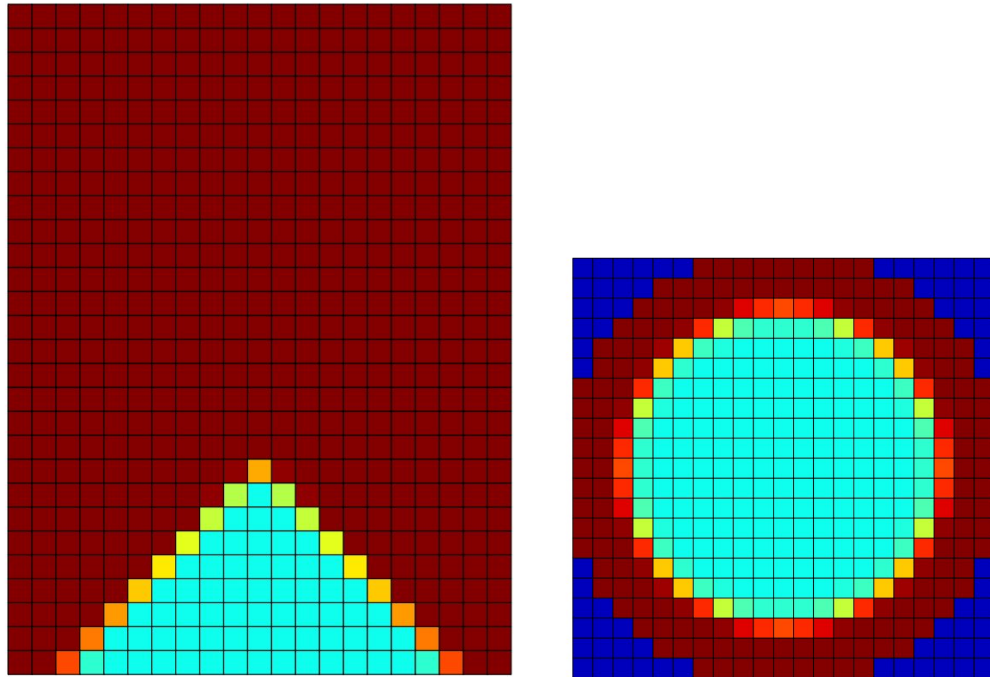


Fig. 7. Central vertical (left) and bottom horizontal (right) cross-sections of the conical PORFLO case for the COOLOCE calculations.

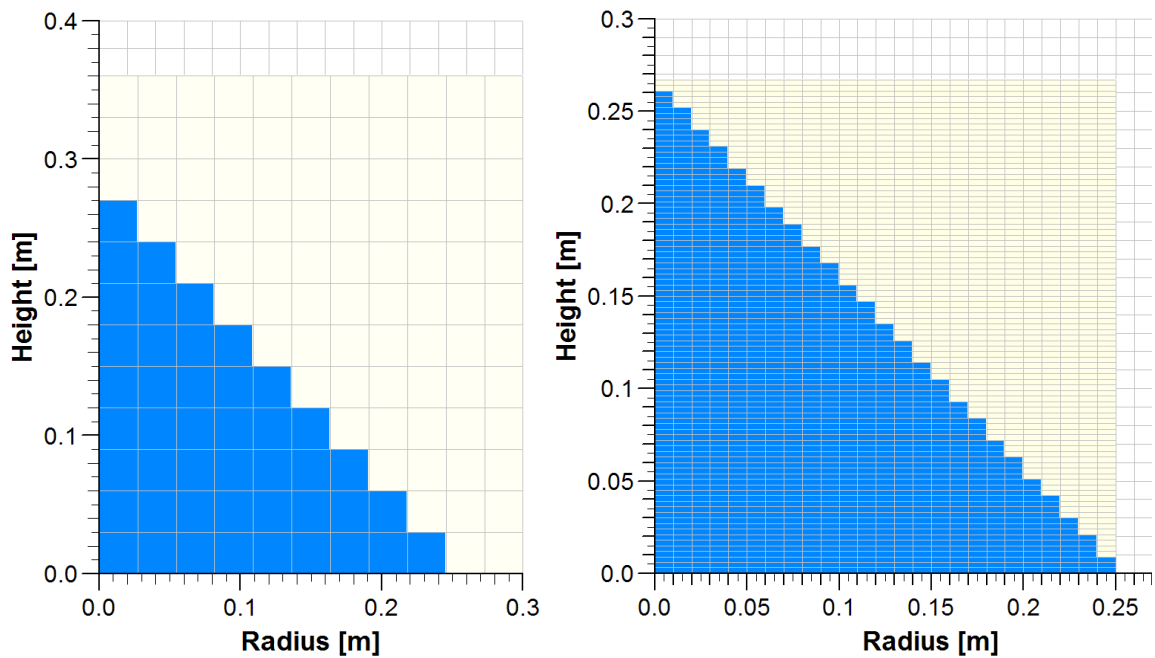


Fig. 8. The MEWA 2D grids for the COOLOCE calculations. The blue area is the particle bed (37% porosity).

Table 9. The simulation set-up for the PORFLO and MEWA calculations of the COOLOCE particle bed.

Simulation parameter	PORFLO (2010)	MEWA (2008)
Coarse grid	21 x 21 x 28 (3D)	11 x 12 (2D)
Dense grid	-	25 x 89 (2D)
Particle bed height	267 mm	270 mm
Particle bed radius	250 mm	270 mm
Particle bed volume	0.01748 m ³	0.02061 m ³
Cell size	30 mm	30 mm
Porosity	~0.36 (calculated based on structure dimensions)	0.37 (given as input)
Pool porosity	0.90	0.99
Particle size	0.8 mm	0.8 mm
Pool particle size	2.0 mm	10.0 mm
Porosity transition zone from particles to pool	Yes	No
Porous friction model	Tung and Dhir	Tung and Dhir
Pool friction model	Tung and Dhir	Tung and Dhir
Upper boundary condition	Pressure, liquid flow only	Pressure, liquid flow only
Wall boundary conditions	Adiabatic, no flow-through	Adiabatic, no flow-through
Heat conductivity model	Imura-Takegoshi/Vortmeyer	Imura-Takegoshi/Vortmeyer
Heated fraction of the porous bed	~100%	100%
Simulation time step	0.01 s	Controlled by the code

5 Simulation results

The results are presented of simulations in which the dryout power is searched by stepwise increases of the heating power. The saturation (void fraction) and flow field inside the porous bed is examined in the pre- and post-dryout conditions. Based on this, estimations on the capabilities of the codes to model the dryout process can be made.

5.1 Cylindrical particle bed

A set of heating power levels applied in the PORFLO simulation is presented in Table 10. For each power level, the minimum saturation (which corresponds to maximum void fraction, $\alpha=1-s_l$) is given. The minimum saturation is a constant value for the steady-state conditions into which the particle bed stabilizes for power densities below the dryout heat flux.

When the heating power corresponds to the minimum dryout power, no coolable steady-state can be established and a transient which will lead to water depletion in the particle bed, and eventually to dryout, occurs. Dryout is considered to occur when the void fraction anywhere in the particle bed permanently reaches 1.0 (saturation reaches 0.0). The accuracy of the dryout power calculation is directly determined by the magnitude of the power increase.

Because it takes some time for the dryout to develop after a power increase to the dryout power, nominal waiting time of 500 s (simulation time at constant power) is applied between the power increases in all the simulations. When the dryout and coolable conditions have been “pin-pointed” with these 500 s power increases, the results have been verified by longer simulations of at least 1000 s.

Table 10. The simulation input power, power density, the resulting minimum saturation and maximum temperature in the PORFLO simulations.

Heating power [kW]	Power density [kW/m ³]	Minimum saturation [-]	Maximum solid temperature [K]
80	1004	0.212	373
90	1129	0.200	373
95	1192	0.0	Transient

The contours of void fraction and particle temperature in coolable conditions are presented in Fig. 9 (2D vertical cross section in the centre of the particle bed). The velocity vectors of vapour and liquid are shown in Fig. 10. In coolable conditions, the void fraction is highest in the upper section of the particle bed which is in accordance with theoretical expectations of void (saturation) profile in the particle

bed. The interpretation of the dryout process as a saturation transient within the particle bed is explained e.g. in Hoffman (1987).

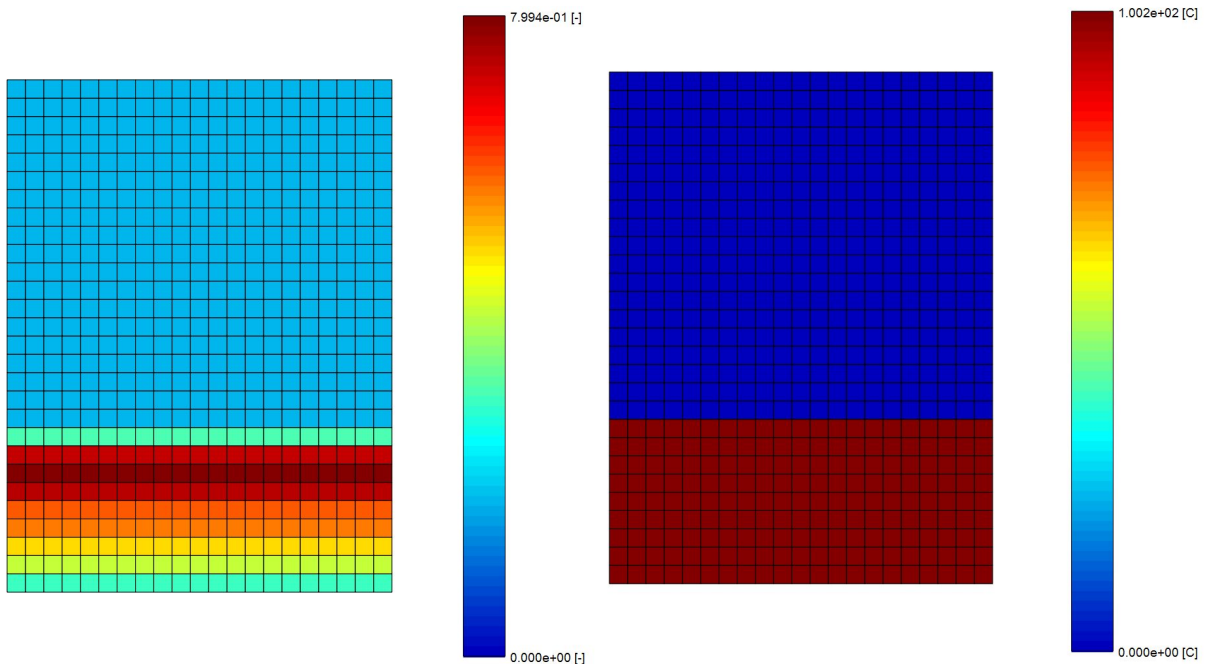


Fig. 9. Void fraction (left) and particle temperature (right) in coolable conditions (90 kW heating power).

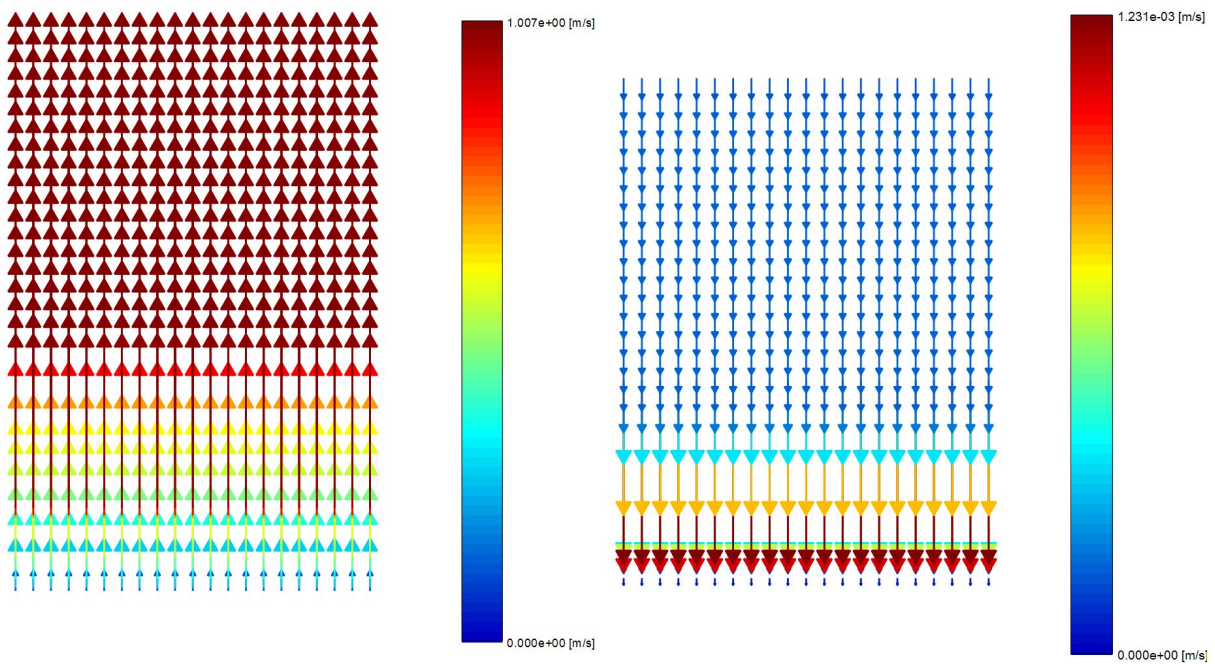


Fig. 10. Gas velocity (left) and liquid velocity (right) in coolable conditions (90 kW heating power).

The void fraction and particle temperature in dryout conditions are illustrated in Fig. 11 and the velocity vectors of gas and liquid in Fig. 12. In this case, dryout

has just been reached and a zero-saturation zone has been formed in the bottom cell row where temperature has started to increase from the saturation temperature. Dryout in the bottom suggests that the applied power is close to the exact dryout power.

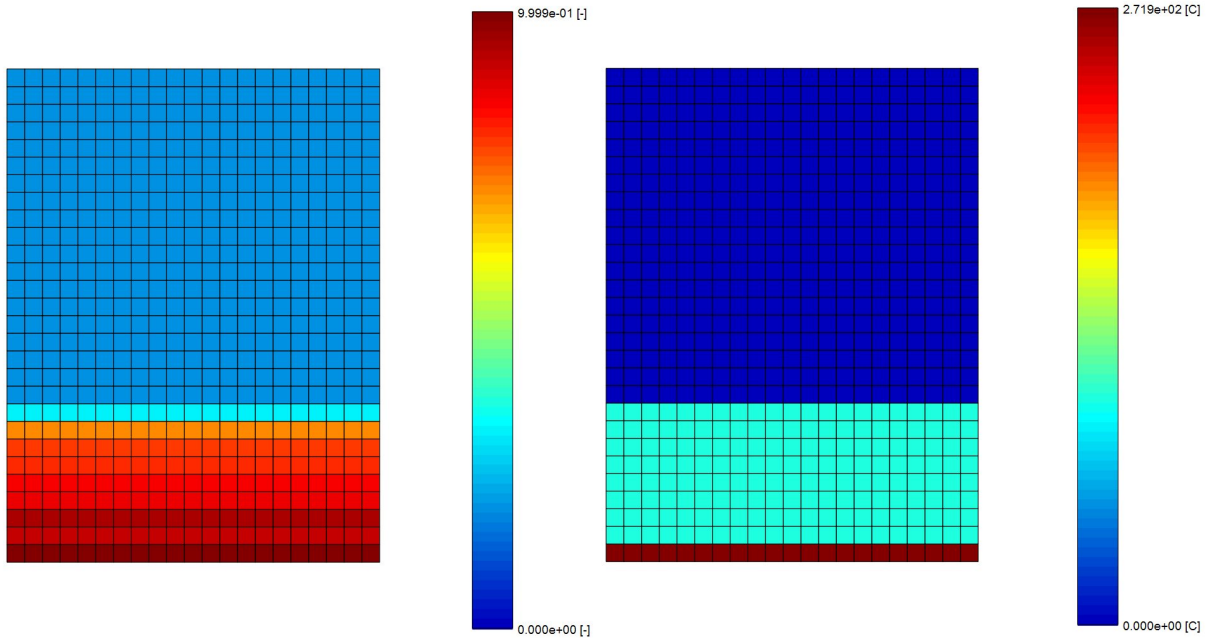


Fig. 11. Void fraction (left) and particle temperature (right) in dryout conditions (95 kW heating power).

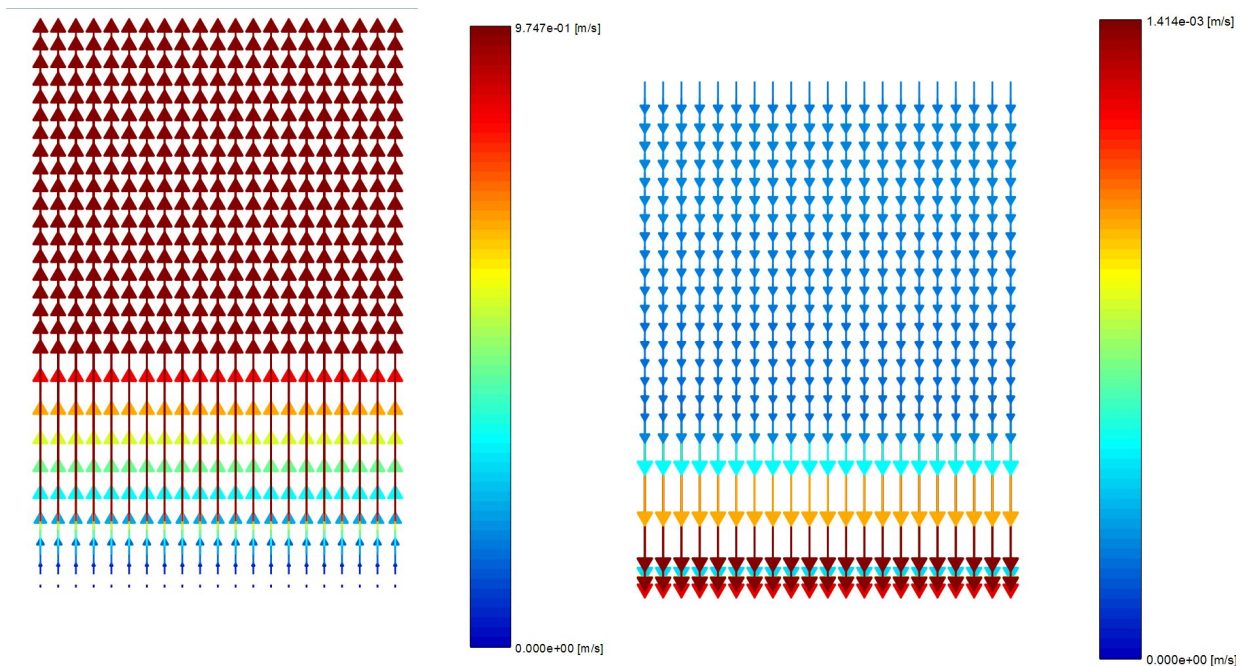


Fig. 12. Gas velocity (left) and liquid velocity (right) in dryout conditions (95 kW heating power).

The development of the saturation profiles towards dryout in the PORFLO simulation is shown in Fig. 13. The power in the presented case is 95 kW which is close to the exact dryout power based on the location of the incipient dryout in the cells near the bottom of the particle bed. The profiles are taken in the centre of the geometry. Because the simulation shows highly symmetric results, the saturation profile is very similar throughout the particle bed and the dryout process can be considered to be effectively one-dimensional. In this sense, the present cylindrical particle bed model in PORFLO approximates the predictions that may be obtained by 1D and 2D models.

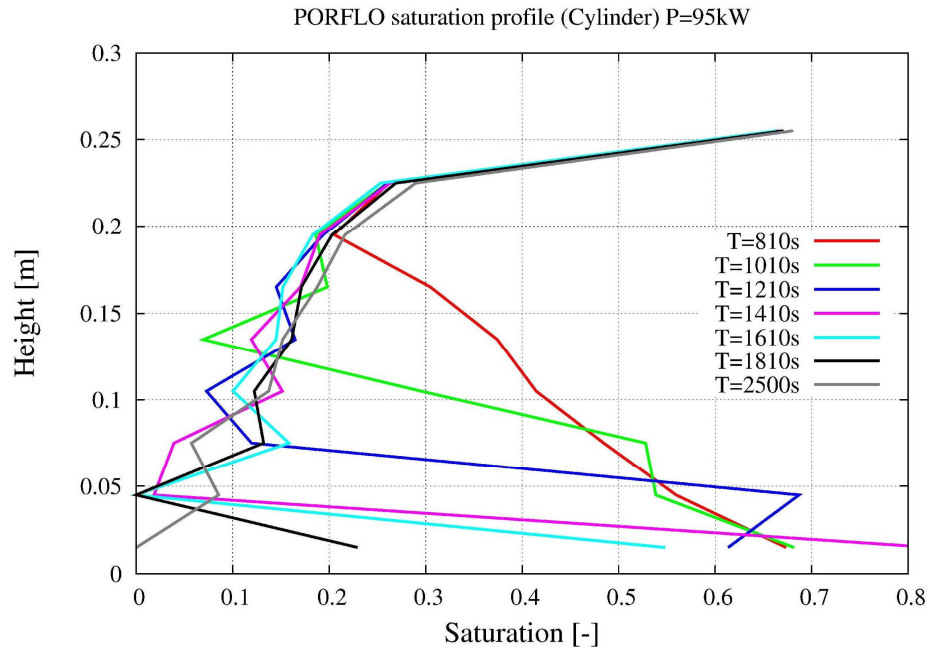


Fig. 13. The saturation development to dryout in the PORFLO simulation of the cylindrical particle bed at constant power.

It is noteworthy that the symmetric result was obtained with the model that utilizes the Reed friction model in both the particle bed and the pool, similarly as in the MEWA code. In this approach, the pool region is also modelled as a particle bed with a high porosity and a large particle size which gives a reduced friction and a high liquid content compared to the particle bed region. No consideration of interfacial friction is included in the Reed model. Because of these issues the pool model can not be considered realistic.

Several of the earlier development versions of PORFLO showed asymmetrical conditions and fluctuating void profiles in the pool area which apparently had an effect on the water infiltration into the particle bed. This, in turn, led to highly asymmetric behavior in the particle bed interior and to dryout in localized regions, even close to the surface of the particle bed. In these earlier versions, separate friction models were tested for the pool region (variations of the Tung and Dhir model) and the particle bed region (Reed model). Currently, the reason to the asymmetrical behavior is somewhat unclear and further studies investigating the effect of the pool dynamics using the latest PORFLO version would be of interest.

For the MEWA simulation, the heating power, the corresponding power density, the minimum saturation and maximum particle temperature for the coarse mesh are given in Table 11. For the dense mesh, this information is given in Table 12. The last row in the tables gives the dryout power.

Table 11. The simulation input power, power density, the resulting minimum saturation and maximum particle temperature in the MEWA simulations (coarse grid).

Heating power [kW]	Power density [kW/m ³]	Minimum saturation [-]	Maximum solid temperature [K]
20	262	0.490	375
25	327	0.453	375
30	393	0.417	375
35	458	0.385	375
40	524	0.355	375
45	589	0.327	375
50	655	0.299	375
55	720	0.272	375
60	786	0.217	375
65	851	0.00	Transient

Table 12. The simulation input power, power density, the resulting minimum saturation and maximum particle temperature in the MEWA simulations (dense grid).

Heating power [kW]	Power density [kW/m ³]	Minimum saturation [-]	Maximum solid temperature [K]
20	262	0.471	375
25	327	0.432	375
30	393	0.392	375
35	458	0.354	375
40	524	0.316	375
45	589	0.270	375
50	655	0.149	375
55	720	0.00	Transient

The contours of liquid saturation and particle temperature in post-dryout conditions for the coarse mesh are presented in Fig. 14. The velocity vectors of vapour are shown in the saturation map and the velocity vectors for liquid in the temperature map. The contours of liquid saturation and particle temperature in post-dryout conditions for the dense mesh are presented in Fig. 15. Note that the saturation map corresponds to the void fraction maps of the PORFLO simulations since $s_l = 1 - \alpha$.

It is seen that prior to dryout, the solid temperature as well as the temperature of the other phases remains close to the saturation temperature. The temperature starts to increase after the first dry spot appears at the power level corresponding to the dryout heat flux. As can be seen in the contour figures, the saturation and particle temperature do not change as a function of the radius of the geometry which means that the system behavior is effectively one-dimensional similarly to the PORFLO results.

A difference of 10 kW in the dryout power predicted by the two MEWA grids indicates that the solution is grid-dependent, and for dryout power estimations in realistic cases, a denser grid should be used.

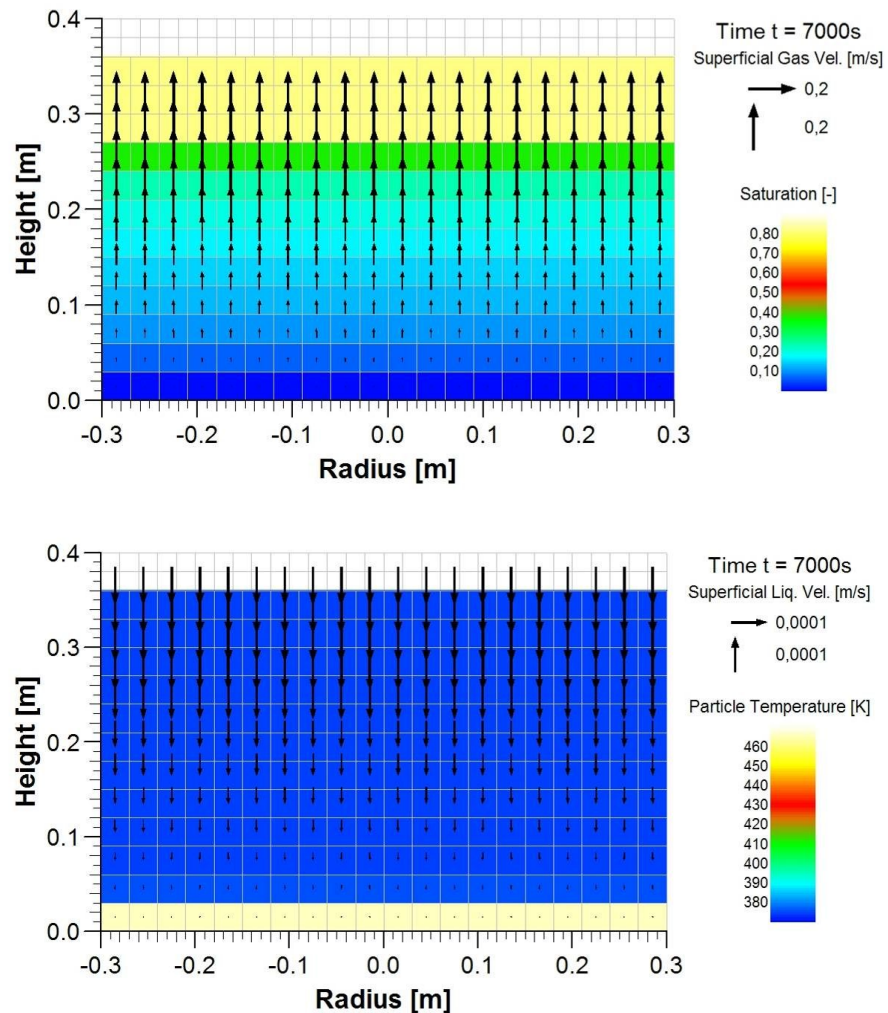


Fig. 14. Saturation (top) and particle temperature (bottom) in post-dryout conditions (MEWA coarse grid).

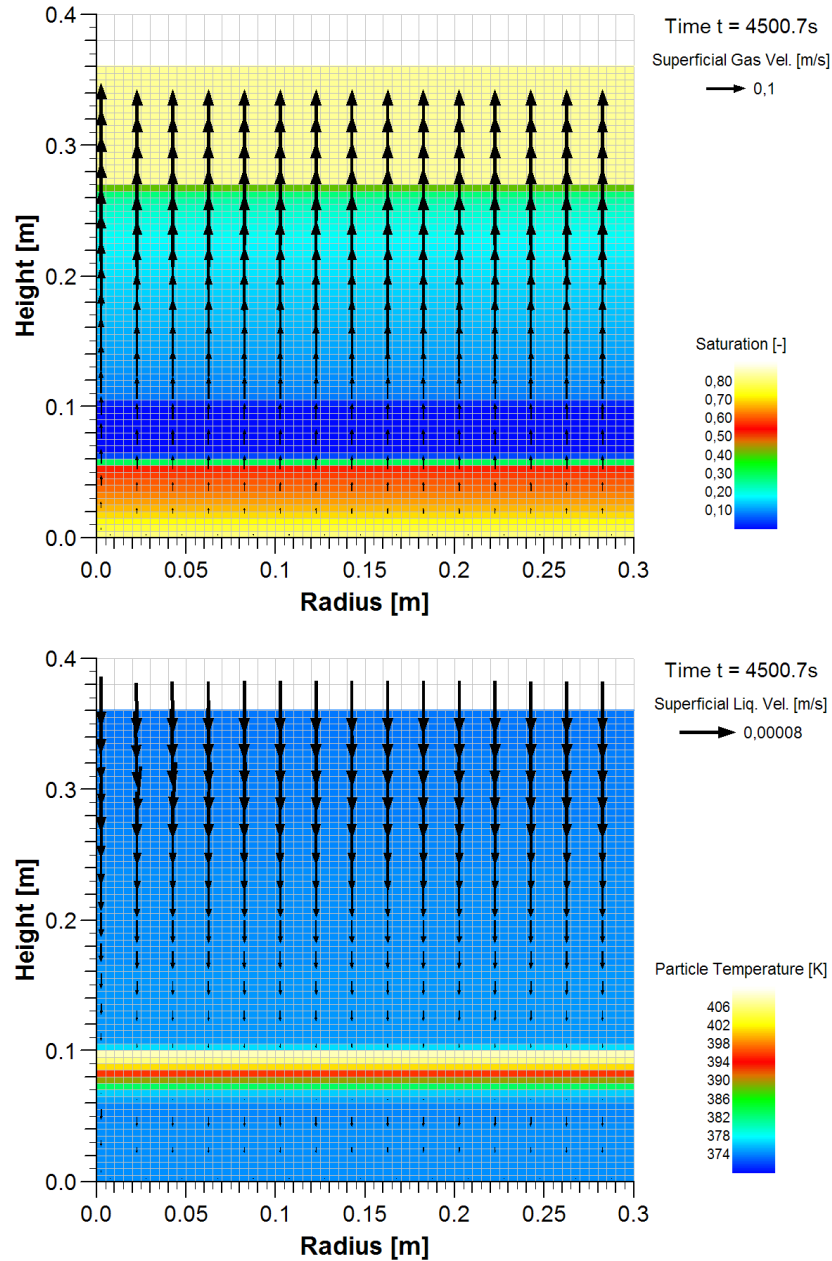


Fig. 15. Saturation (top) and particle temperature (bottom) in post-dryout conditions (MEWA dense grid).

The saturation profiles within the particle bed during the development towards dryout (water depletion inside the particle bed) are plotted in Fig. 16. The result is typical to a top-flooded bed which is heated by a constant power slightly exceeding the dryout power. It is also seen that the general development towards dryout is rather similar in the PORFLO results (Fig. 13) suggesting that PORFLO is a potentially useful tool for detailed simulations of particle bed coolability as a result of the code development.

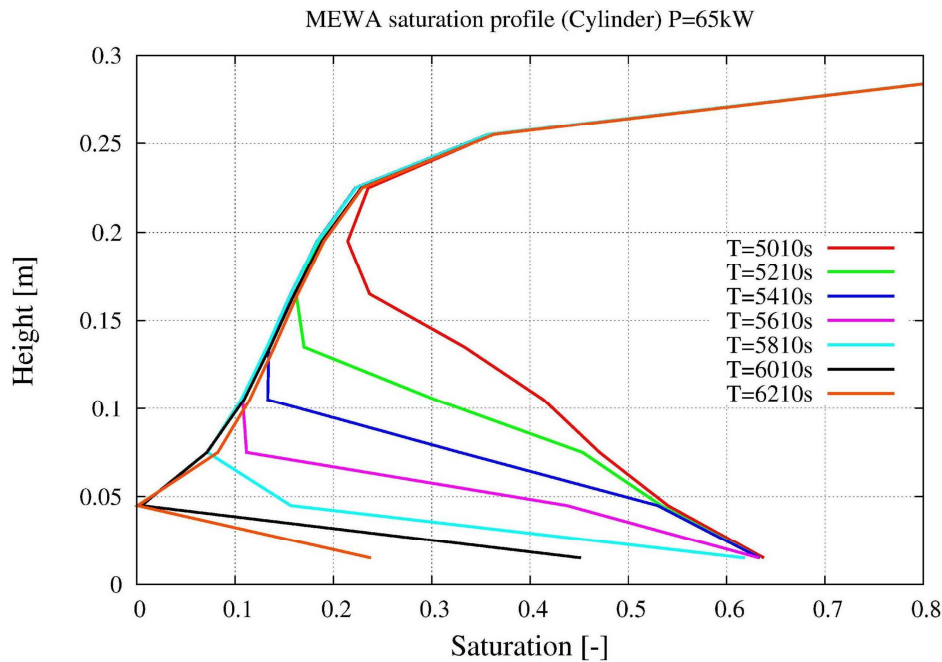


Fig. 16. The saturation development to dryout in the MEWA coarse mesh simulation of the cylindrical particle bed at constant power.

5.2 The COOLOCE particle bed

The heating power levels in the PORFLO simulation of the COOLOCE geometry and the resulting minimum saturation and maximum solid temperature are presented in Table 13.

Table 13. The simulation input power, power density, the resulting minimum saturation and maximum solid temperature in the PORFLO simulations.

Heating power [kW]	Power density [kW/m ³]	Minimum saturation [-]	Maximum solid temperature [K]
15	858	0.139	373
20	1144	0.111	373
25	1430	0.0872	373
30	1716	0.051	373
35	2002	0.0	Transient

The void fraction distribution inside the particle bed in pre-dryout conditions is illustrated in Fig. 17. The highest void is observed in the central topmost cell of the cone. In the beginning of the simulation, the cone is surrounded by pure liquid. Steam travels upwards after the heating is started as seen in the void fraction in the pool region above the particle bed. The void fraction distribution in post-dryout condition is shown in Fig. 18. The vectors of gas and liquid velocities at 25 kW power (coolable) are presented in Fig. 19 and Fig. 20,

respectively. The velocity field is very similar in post-dryout conditions at 35 kW just after dryout has been reached.

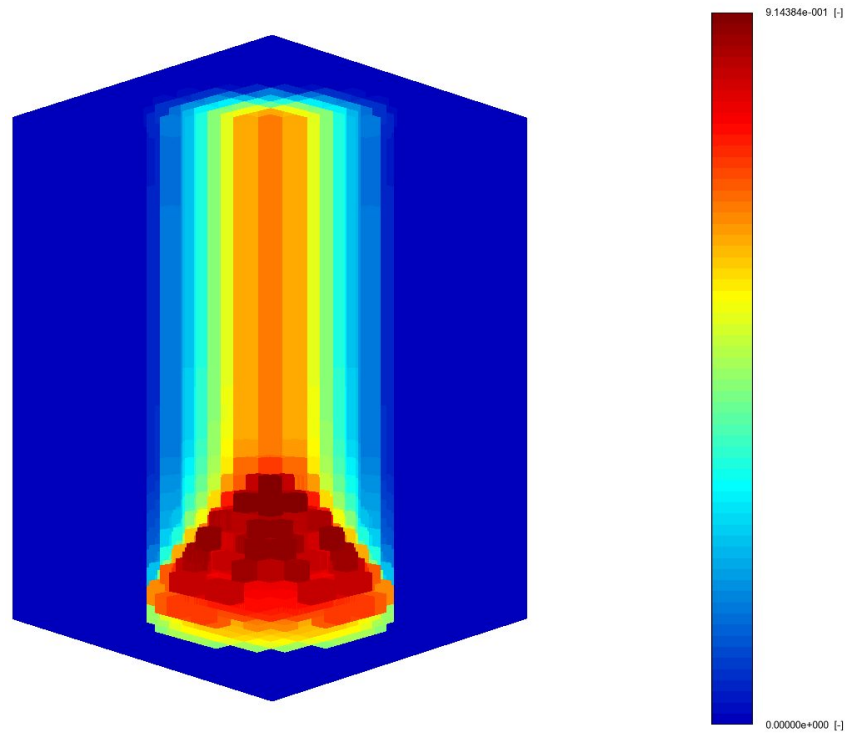


Fig. 17. Void fraction in the PORFLO simulation in pre-dryout conditions at the power level of 25 kW.

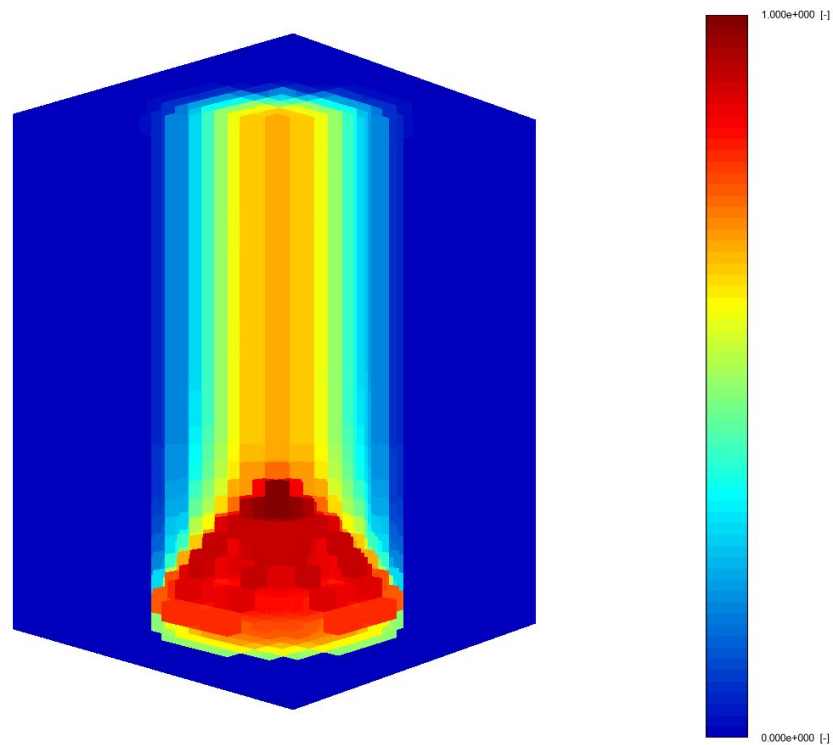


Fig. 18. Void fraction in the PORFLO simulation in post-dryout conditions at the power level of 35 kW.

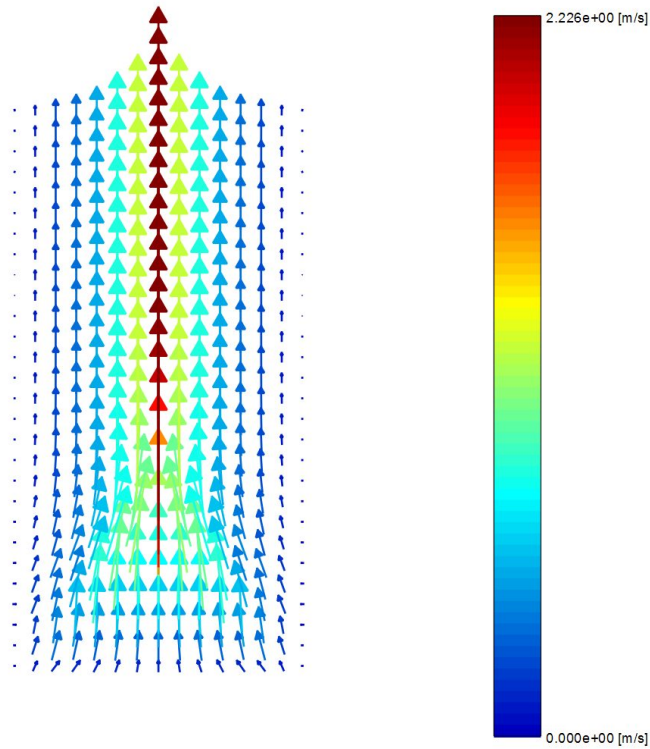


Fig. 19. The vectors of gas velocity in the PORFLO simulation of the COOLOCE particle bed in pre-dryout conditions at the power of 25 kW.

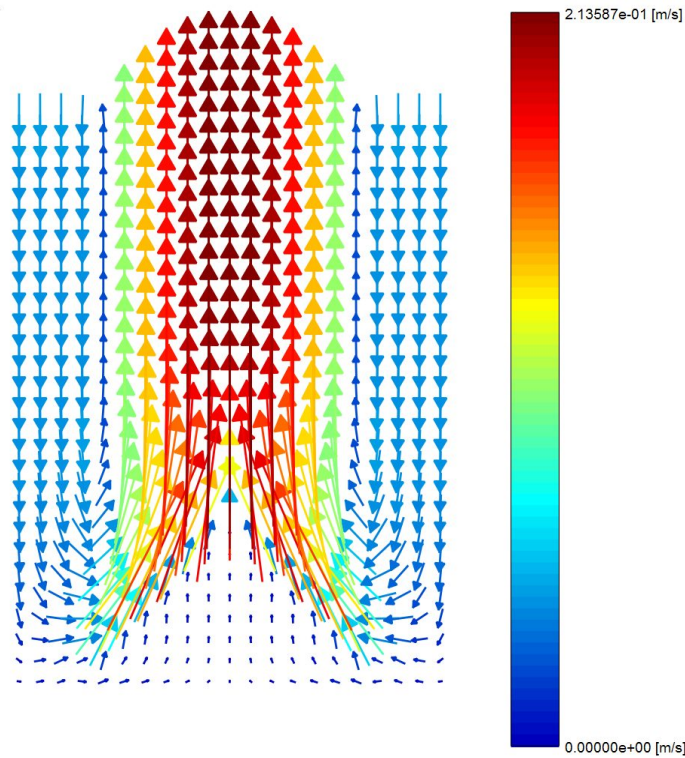


Fig. 20. The vectors of liquid velocity in the PORFLO simulation of the COOLOCE particle bed in pre-dryout conditions at the power of 25 kW.

The saturation profiles during the development towards dryout in the conical particle bed are shown in Fig. 21. The profiles are taken from the centre of the

cone where the dryout is first seen. Because of the complexity of the geometry and the multi-dimensional flow configuration, the saturation profiles change depending on the location inside the particle bed. This means that no universal saturation profile such as in the cylindrical case exist for the conical case. In this case, dryout is by definition local while in the cylindrical top flooding configuration, it may be considered global, i.e. the full cross-section of the particle bed is dried out at the same time.

The lowest saturation (highest void) is located in the topmost cells throughout the simulation. This appears to be a reasonable result because the lateral flows from the sides of the cone maintain the liquid reservoir in the lower bottom parts of the cone. On the other hand, the highest mass flux of vapour inside the particle bed is present in the top central part of the cone. The mass flux increases according to the volumetric heating power. As a result, this zone is dried out when the vapour flow is high enough to replace the liquid flow in the full cross-section of the conical geometry.

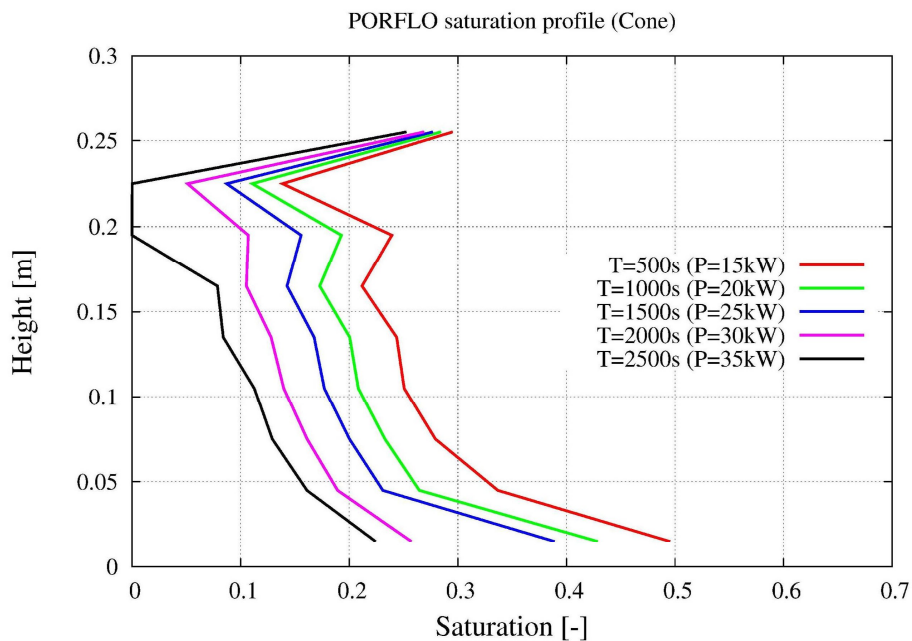


Fig. 21. Saturation development to dryout in the PORFLO simulation of the COOLOCE particle bed (increasing heating power).

The heating power levels in the simulation and the corresponding minimum saturation and maximum solid temperature in the MEWA simulations are presented in Table 14 (coarse grid) and Table 15 (dense grid). The coarse grid case reaches dryout with the input power of 260 kW, and the dense grid at 20 kW.

Table 14. The simulation input power, power density, the resulting minimum saturation and maximum particle temperature in the MEWA simulations (coarse grid).

Heating power [kW]	Power density [kW/m ³]	Minimum saturation [-]	Maximum solid temperature [K]
200	9703	0.211	379
210	10188	0.188	379
220	10673	0.160	380
230	11159	0.118	381
240	11644	0.0751	383
250	12129	0.0165	416
260	12614	0.00494	681

Table 15. The simulation input power, power density, the resulting minimum saturation and maximum particle temperature in the MEWA simulations (dense grid).

Heating power [kW]	Power density [kW/m ³]	Minimum saturation [-]	Maximum solid temperature [K]
10	485	0.215	392
15	728	0.101	392
20	970	0.0	Transient

The contours of saturation and solid particle temperature of the MEWA simulation at 250 kW total power are presented in Fig. 22. The vectors of liquid velocity are indicated in the temperature map. Fig. 23 presents the corresponding graphs for the dense grid case.

In the dense grid case, the dryout power predicted by the simulation is remarkably lower than in the coarse grid case. Previous analysis and the first results of the COOLOCE experiments (Takasuo et al. 2010) indicate that the power of 20 kW is within the reasonable range for the expected dryout power of the conical system.

The measured dryout power in the COOLOCE-1 experiment was 46 kW at 1.9 bar pressure (according to the power control). In the COOLOCE-2 experiment, the dryout power was 43.8 kW at 1.6 bar pressure. Taking into account the heat losses of the test facility, the dryout power values are approximately 40 kW for COOLOCE-1 and 38 kW for COOLOCE-2. Apparently, the resolution of the MEWA coarse mesh is not adequate to capture the onset of local dryout correctly. Nevertheless, the approximate dryout location predicted by the PORFLO and MEWA codes correspond to the one measured in the experiments.

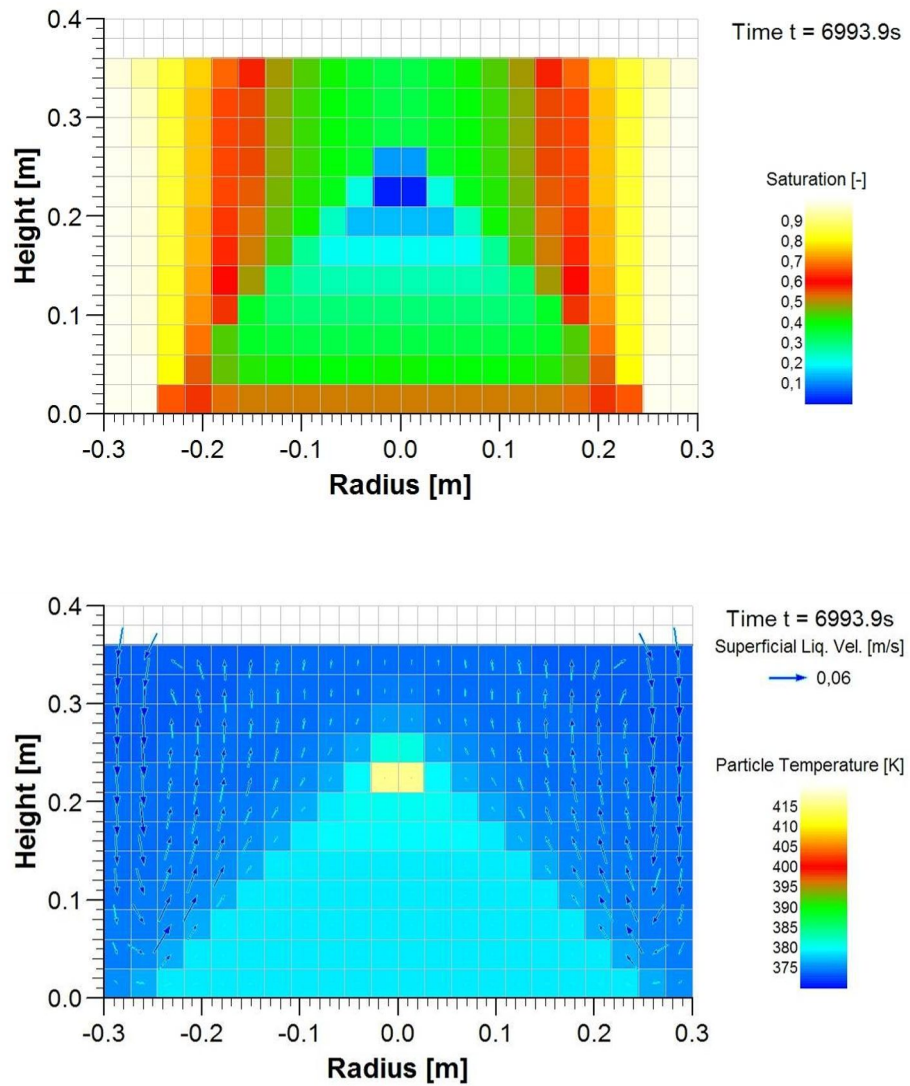


Fig. 22. Saturation (top) and particle temperature with liquid velocity vectors (bottom) just after dryout has been reached (MEWA coarse grid).

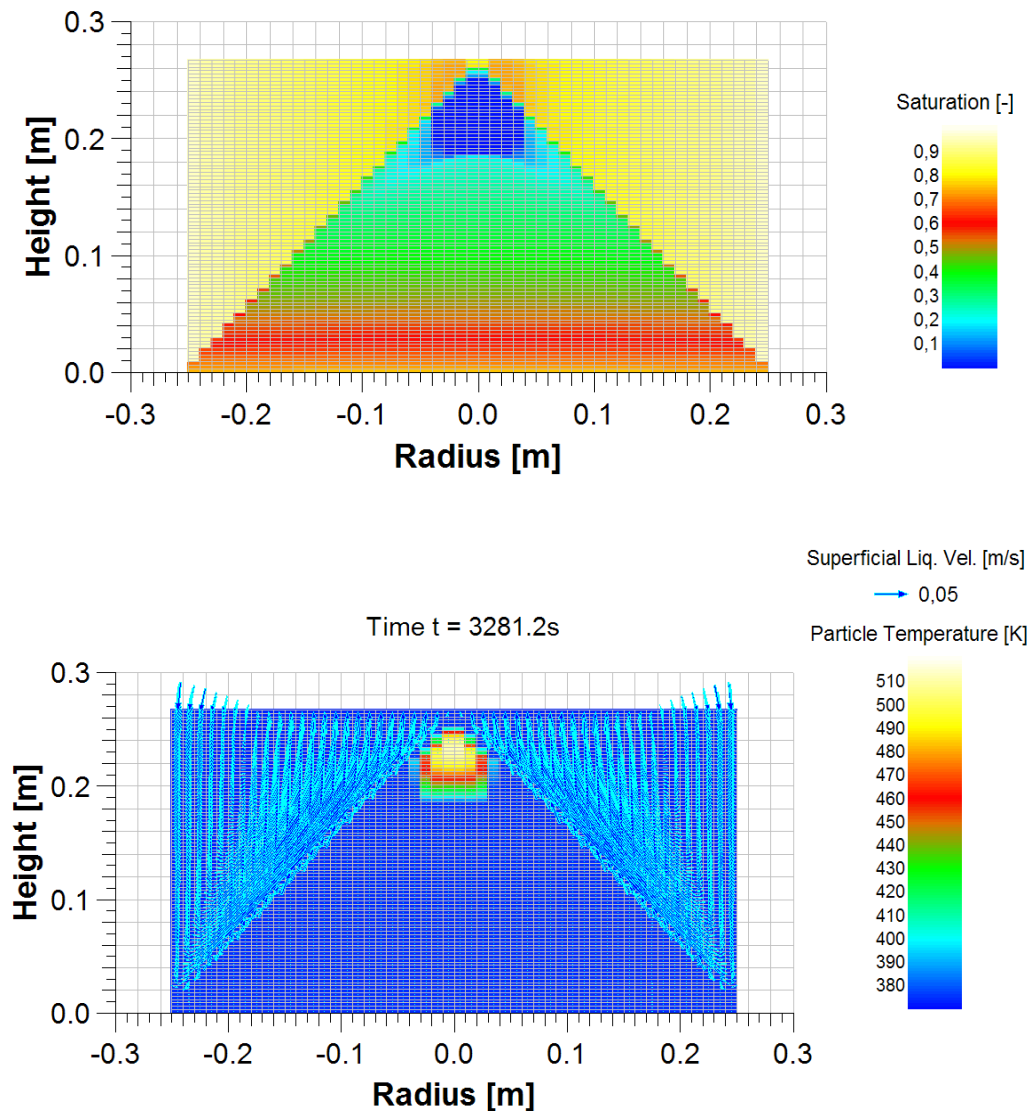


Fig. 23. Saturation (top) and particle temperature with liquid velocity vectors (bottom) just after dryout has been reached (MEWA dense grid).

The saturation profiles at different power levels (200 kW – 270 kW) in the COOLOCE simulation using MEWA are plotted in Fig. 24. Contrary to the cylindrical case (Fig. 16) and similarly to the PORFLO simulation, dryout is initiated in the topmost cells of the geometry, with very little change of the saturation profile at different power levels before and after dryout. During the stepwise power increase, the steam generation (boiling rate) increases accordingly until the steam flux is great enough for the formation of the first dry zone. This occurs in the top region of the cone because water infiltration through the sides of cone ensures that coolant is available near the bottom of the geometry.

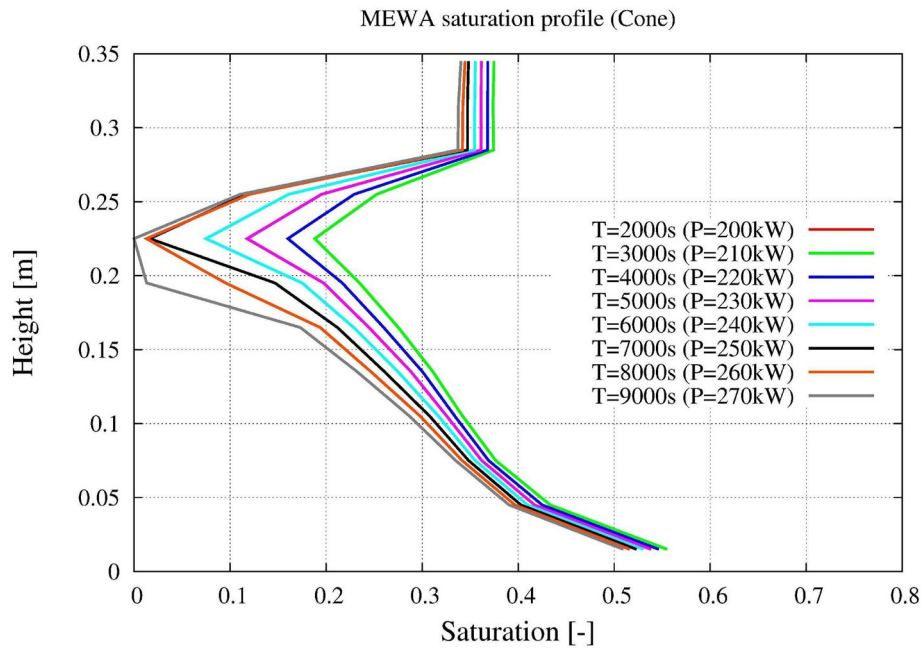


Fig. 24. The saturation development to dryout in the MEWA coarse grid simulation of the conical particle bed (increasing heating power).

6 Conclusions

The PORFLO code has been set-up for calculating fluid flow and heat transfer in porous debris beds that generate decay heat. For this purpose, appropriate heat transfer and friction models have been selected and incorporated into the code. During the work, the solutions of conservation equations implemented into the code have been completely revised as part of the application-independent PORFLO code development.

A 3D model of the new COOLOCE test facility investigating a conical (heap-like) particle bed has been generated, and test simulations have been run. Top flooding cases with a simple cylindrical particle bed have also been tested. Comparisons of the void fraction development in the particle bed interior during the simulations to theoretical expectations and 2D simulations by MEWA have been done. The results suggest that the main features of the dryout process of the particle bed are qualitatively well captured by the latest version of the PORFLO code. However, discrepancies still appear in the predictions of dryout power by the different codes which should be further investigated by e.g. grid sensitivity studies and comparisons to the COOLOCE experimental results.

In addition, it would be of interest to further investigate the possibilities to combine the two-phase flow models for the particle bed and the water pool above the bed in order to develop physically detailed 3D models for both the particle bed and the pool. This is because the friction model of the pool flow seems to have an effect on the water infiltration into the particle bed in the case of cylindrical bed. In the present model of the cylindrical bed in both codes, the pool region is

modelled as a type of high-porosity particle bed with no gas-liquid friction. The model produces realistic saturation profiles for a top-flooded bed while the model which includes the interfacial friction in the pool region does not seem to capture the dryout process correctly. Since interfacial friction is expected to play an important role in two-phase flow in the pool and it might be expected that a model including the gas-liquid friction would produce better results than the high-porosity pool approximation, this is a rather curious observation. Simulations with more variations of the friction models and the grid are needed to clarify the issue. For the conical particle bed, the pool conditions appear to be clearer as the gas is lead upwards above the particle bed and liquid flows down near the perimeter of the geometry, according to the model utilizing the Tung and Dhir interfacial friction.

References

- Buck, M., Pohlner, G., Rahman, S. Documentation of the MEWA code. 2009. IKE Institut für Kernenergetik und Energiesysteme, Universität Stuttgart. August 2009.
- Bürger, M., Buck, M., Schmidt, W., Widmann, W. 2006. Validation and application of the WABE code: Investigations of constitutive laws and 2D effects on debris coolability. *Nuclear Engineering and Design* 236 (2006), p. 2164-2188.
- Hofmann, G. 1987. Dryout in very deep particulate beds, *Nuclear Engineering and Design* 99 (1987), p. 177–185.
- Hovi, V. 2008. Calculations of Boiling Two-Phase Flow Using a Porous Media Model. Master's Thesis. Lappeenranta University of Technology. 112 p.
- Hovi, V., Ilvonen, M. 2010. PORFLO Simulations of Loviisa Horizontal Steam Generator. VTT Research Report, VTT-R-01406-10, Espoo. 34 p.
- Ilvonen, M., Hovi, V., Inkinen, P. 2010. PORFLO development, applications and plans in 2008-2009. VTT Research Report, VTT-R-01414-10, Espoo. 28 p.
- Imura, S., Takegoshi, E. 1974. Effect of Gas Pressure on the Effective Thermal Conductivity of Pack Beds. *Heat Transfer Japanese Research*, Vol. 3, No. 4, 13 p.
- Lee, K., Ryley, D.J. The evaporation of water droplets in superheated steam. *ASME Journal of Heat Transfer*, 445-456, 1968.

Lienhard, J.H., Dhir, V.K. Extended Hydrodynamic Theory of the Peak and Minimum Pool Boiling Heat Fluxes. National Aeronautics and Space Administration Report NASA-CR-2270, July, 1973.

Lindholm, I., Holmström, S., Miettinen, J., Lestinen, V., Hyvärinen, J., Pankakoski, P., Sjövall, H., 2006. Dryout Heat Flux Experiments with Deep Heterogeneous Particle Bed. Nuclear Engineering and Design, 236, 2060-2074.

Rohsenow, W.M. A Method of Correlating Heat Transfer Data for Surface Boiling Liquids. Trans. ASME, 74, 969, 1952.

Schmidt, W. 2004. Influence of Multidimensionality and Interfacial Friction on the Coolability of Fragmented Corium. Doctoral Thesis. Institut für Kernenergetik und Energiesysteme. IKE 2 – 149. ISSN-0173-6892.

Takasuo, E., Holmström, S., Kinnunen, T., Pankakoski, P.H., Hosio, E., Lindholm, I. 2010. The effect of lateral flooding on the coolability of irregular core debris beds. Nuclear Engineering and Design (2010). doi:10.1016/j.nucengdes.2010.04.033

Takasuo, E. Kinnunen, T., Pankakoski, P.H., Holmström, S. Description of the COOLOCE test facility – Conical particle bed. VTT Research Report VTT-R-08956-10. Espoo, 2010. 18 p.

Tung, V.X. and Dhir, V.K., 1988. A Hydrodynamic Model for Two-Phase Flow through Porous Media. International Journal of Multiphase Flow, 14, No. 1, p. 47-65.

Tutu, N., Ginsberg, T., Chen, J., 1984. Interfacial drag for two-phase flow through high permeability porous beds. Journal of Heat Transfer 106, p. 865-870.

Vortmeyer, D. 1978. Radiation in Packed Solids. 6th International Heat Transfer Conference, Toronto, Canada, 1978.